Dynamics of Entangled Associating Polymers with Large Aggregates

A. N. Semenov

Department of Applied Mathematics, University of Leeds, Leeds LS2 9JT, U.K., and Department of Physics, Moscow State University, Moscow 117234, Russia

Michael Rubinstein*

Department of Chemistry, University of North Carolina, Chapel Hill, North Carolina 27599-3290

Received October 10, 2001; Revised Manuscript Received January 16, 2002

ABSTRACT: We develop a theory for the dynamics in entangled solutions of associating polymers with many stickers per chain. The stickers strongly associate and form large aggregates that control both the equilibrium structure of the system and its dynamics. The association results in formation of micelles that separate macroscopically yielding a reversible gel phase of interconnected, closely packed micelles. We identify two mechanisms for stress relaxation: (a) polymer chain diffusion and (b) positional rearrangements of the micelles, and predict that the second process is exponentially slower than chain diffusion. Hence, a polymer chain may diffuse through many of its gyration radii during the terminal stress relaxation time. We predict an exponentially strong concentration dependence of the micellar gel viscosity typically involving one or more anomalous regimes where the viscosity is decreasing with concentration. We also show that the chain self-diffusion constant decreases exponentially with concentration in the strongly entangled regime (entangled spacers connecting the stickers).

1. Introduction

A copolymer incorporating both soluble fragments and a small fraction of insoluble chemical groups (stickers) that strongly attract each other is often called associating polymer. Different chemical units may be used as stickers depending on the solvent: e.g., hydrophobic alkyl fragments in aqueous solutions, polar or ionic groups in organic solvents. The stickers form stable aggregates in solutions or in melts. The number m of stickers per aggregate (aggregation number) depends on the size of the sticker groups and on their attraction energy, and may vary from just 2 to about 100.[1−5] The aggregates serve as temporary junction points for reversible gel structures of associating polymers defining their high viscosity, strong viscoelasticity, and unusual (and useful) rheological properties.

In a recent series of papers[6−8] we have developed a theory for the dynamics of main-chain associating polymers with many stickers per chain ($f \gg 1$) and with pairwise association ($m = 2$), both in the unentangled and entangled regimes. The dynamics of telechelic polymers with two end-stickers per macromolecule ($f = 2$) and with large aggregates ($m \gg 1$) was considered earlier.[9] The aim of the present paper is to bridge the gap between the two approaches. We consider dynamics of associating polymers with many ($f \gg 1$) stickers per chain forming large ($m \gg 1$) aggregates. One of the important effects elucidated in refs. 7 and 8 is a substantial slowing down of the dynamics due to strong correlations between association (formation of a bond between two stickers) and dissociation events. This effect is important in the so-called strong association regime when the fraction of unassociated (free) stickers is small. This is the typical regime for most associating polymers and will be considered below. In particular, we calculate the concentration dependence of the viscosity and other dynamic quantities and find a number of anomalous regimes with both the viscosity and the polymer self-diffusion constant decreasing with concentration, or with the stress relaxation time much longer than the relaxation time of chain conformations.[10]

In section 2 we introduce the model and describe the equilibrium structure of reversible gels with large aggregates. The gels are formed by interconnected flowerlike micelles. We discuss the structure of the micelles, their interaction, and estimate the elastic modulus of the gel. In section 3 we analyze the dynamics of stickers and of associating chains with entanglements. The dynamics of positional rearrangements of the micelles are considered in section 4, which is followed by the summary of the main results regarding concentration dependencies of relaxation times, the self-diffusion constant and the viscosity. The paper is concluded by the discussion of the main predictions.

2. The Model and Equilibrium Properties

2.1. The Model. Consider a solution of flexible linear associating macromolecules. Each macromolecule is a linear soluble polymer chain with f stickers attached to it or incorporated in it (Figure 1a). The mean number of soluble monomers per sticker is l and the degree of polymerization of the soluble part of the chain is $N \simeq lf$. Assume that the number of stickers per chain is large, $f \gg 1$, and the average number of monomers in a soluble spacer between stickers is also large, $l \gg 1$. The stickers strongly attract each other and their aggregates are stable even at low polymer concentrations. Note that a sticker is not necessarily just one monomer. A sticker can be a relatively short insoluble block of l' monomers, $l' \ll l$. We will treat the aggregation number m as an 'input' parameter, assuming large aggregates, $m \gg 1$.

It is not impossible to predict m for a particular chain structure, say, for a chain of alternating long soluble (l) and short insoluble (l') blocks. In this case, aggregates are similar to block copolymer micelles that have been studied in detail in the past.[11,12] The aggregation

* To whom correspondence should be addressed.

10.1021/ma0117965 CCC: $22.00
Published on Web 04/30/2002

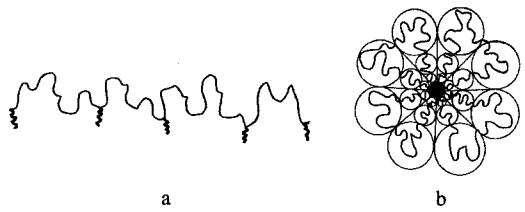

a b

Figure 1. (a) An associating polymer consists of a soluble backbone and *f*-associating groups (stickers) represented by thick lines. The average number of statistical segments per soluble spacer between stickers is l. (b) A flowerlike micelle consists of a core formed by m associating groups (stickers) and a corona of loops (petals). Open circles represent correlation volumes.

number of a block copolymer micelle is a function of l, l' and the attraction energy. However, the calculation of aggregation number is not always useful, as it is more difficult to measure the attraction energy than to deduce the aggregation number from experimental data. Yet in some regimes, the energetic dependence of m is weak.[13]

2.2. Structure of a Flower Micelle. The equilibrium structure of the system is similar to that of telechelic chains considered in ref 9. At low concentrations chains form flowerlike micelles. Each micelle consists of a core (an aggregate) and is decorated by a corona of soluble loops (l monomers per loop) yielding a 'flower' (Figure 1b). A compact core of radius r_a in the center of a flower micelle is formed by m associated stickers. Stickers are strongly bound together in the aggregate. Dissociation of just one sticker costs high energy $\epsilon k_B T$, with $\epsilon \gg 1$.

The core is surrounded by the corona of soluble l-fragments which is locally similar to a star with $2m \gg 1$ arms. We assume the good solvent conditions for l-fragments and apply the relevant scaling results obtained for multiarm stars in refs. 14−17 (see also ref 9). The correlation blobs of each arm are confined to cones with a solid angle $\sim 1/m$. The correlation length, ξ (the size of a correlation blob), increases with the distance r to the center of micelle as the radius $r/\sqrt{m}$ of these cones.

$$\xi \approx \frac{r}{\sqrt{m}} \tag{1}$$

In a good solvent for soluble l-fragments the size ξ of a correlation blob is related to the number of monomers g in it

$$\xi \approx b g^{\nu} \tag{2}$$

where the Flory exponent $\nu \cong 0.59$. Here and below, we assume that the chains are flexible with statistical length b and monomer volume $v \approx b^3$. Concentration (volume fraction), ϕ, of soluble monomers is high near the core decaying away from it. It can be estimated from the condition of correlation blobs densely packing the corona of the micelle.

$$\phi(r) \approx \frac{g b^3}{\xi^3} \approx \left(\frac{b}{\xi}\right)^{(3\nu-1)/\nu} \approx \left(\frac{b\sqrt{m}}{r}\right)^{(3\nu-1)/\nu} \simeq \left(\frac{b\sqrt{m}}{r}\right)^{1.3} \tag{3}$$

We may expect that $\phi(r_a) \approx 1$, hence, the radius of the aggregate at the core of the micelle is

$$r_a \approx b\sqrt{m} \tag{4}$$

The radius of an isolated flower is estimated from the condition that each loop contains l monomers. The number of monomers, g, in a correlation blob of a loop increases with the distance r from the center of the flower. Therefore, summing the number of monomers g per blob over all blobs in a loop should give the number of monomers l per loop.

$$\int_{r_a}^{R^*} g \frac{\mathrm{d}r}{\xi} \approx l \tag{5}$$

The integral can be evaluated using eqs 1 and 2.

$$\int_{r_a}^{R^*} g \frac{\mathrm{d}r}{\xi} \approx \int_{r_a}^{R^*} \left(\frac{\xi}{b}\right)^{1/\nu} \frac{\mathrm{d}r}{\xi} \approx \int_{r_a}^{R^*} \left(\frac{r}{b\sqrt{m}}\right)^{1/\nu - 1} \frac{\mathrm{d}r}{b} \approx \sqrt{m}\left(\frac{R^*}{b\sqrt{m}}\right)^{1/\nu} \approx l \tag{6}$$

Therefore, the radius of an isolated micelle is

$$R^* \approx b l^{\nu} m^{(1-\nu)/2} \simeq b l^{0.59} m^{0.21} \tag{7}$$

Of course, we assume that $R^* \gg r_a$, i.e., the number of monomers l per spacer between stickers is much larger than the square root of the aggregation number.

$$l \gg m^{1/2} \tag{8}$$

The average polymer volume fraction in an isolated flower is

$$\phi^* \approx \frac{m l b^3}{(R^*)^3} \approx \left(\frac{\sqrt{m}}{l}\right)^{3\nu-1} \simeq \left(\frac{\sqrt{m}}{l}\right)^{0.77} \tag{9}$$

The corona free energy, $\mathcal{F}_c$, is due to (i) excluded volume interactions of monomers (*osmotic* free energy) and (ii) radial elongation of l-fragments (*elastic* free energy). The two contributions are of the same order in an isolated micelle and are proportional to the total number of correlation blobs (the number of correlation blobs per arm times the number of arms per micelle m).

$$\mathcal{F}_c \approx k_B T m \int_{r_a}^{R^*} \frac{\mathrm{d}r}{\xi} \approx k_B T m \int_{r_a}^{R^*} \sqrt{m} \frac{\mathrm{d}r}{r} \approx k_B T m^{3/2} \ln \frac{R^*}{r_a} \tag{10}$$

Obviously the dissociation energy, $\epsilon k_B T$, must be higher than $\partial \mathcal{F}_c / \partial m$, otherwise the core would be globally unstable with respect to sticker dissociation, i.e.

$$\epsilon \gtrsim \frac{1}{k_B T} \frac{\partial \mathcal{F}_c}{\partial m} \approx m^{1/2} \tag{11}$$

neglecting the logarithmic factor.

The flower micelles attract each other, and the attraction energy is high if $m \gg 1$ (this energy is proportional to $m^{5/6}$).[9] Hence, the flower micelles phase separate in dilute solution ($\phi < \phi^*$) and form a phase of densely packed micelles in equilibrium with a nearly pure solvent phase. The micelles are connected by soluble bridges (see below), i.e., this phase is a reversible gel. Therefore, the reversible gelation in the system is accompanied by phase separation. The *gelation concentration* is the overlap concentration of micelles ϕ^*, as defined in eq 9. The gel phase at $\phi > \phi^*$ is the subject of the present work.

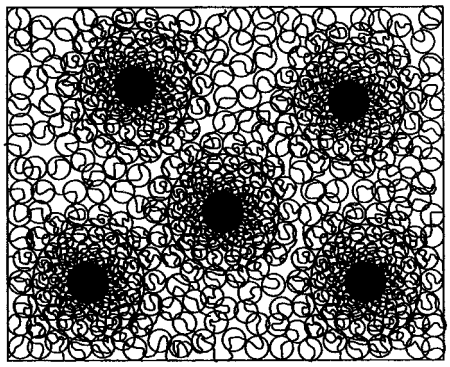

Figure 2. A network of interconnected micelles at concentration $\phi > \phi^*$. Cores of micelles are represented by black circles. Concentric open circles around the cores represent inner parts of micelles of radius R_s. Other open circles represent correlation volumes. Correlation volumes in the outer part of micelles have the same size. In the inner parts of micelles the size of correlation volume decreases toward micellar cores, as in isolated micelles at concentrations $\phi < \phi^*$.

At higher concentrations ($\phi > \phi^*$) the micellar size R follows the scaling law that can be derived from the dense packing condition for micelles $\phi \approx mlb^3/R^3$.

$$R \approx b\left(\frac{lm}{\phi}\right)^{1/3} \approx R^*\left(\frac{\phi^*}{\phi}\right)^{1/3}, \quad \phi > \phi^* \tag{12}$$

Here, we assume that aggregates are fairly stable and the aggregation number m is concentration independent.

The corona size at higher concentrations is smaller than R^* with l-fragments less stretched. In fact, only the inner parts of the soluble fragments (i.e. the parts close to the stickers) in the region $r_a < r < R_s$ are as stretched as in an isolated flower micelle (see Figure 2). The monomer density profile $\phi(r)$ in this region is still defined by eq 3. The crossover length R_s is obtained from eq 3 by equating the concentration at R_s to the solution concentration $\phi(R_s) \approx \phi$.

$$R_s \approx b\sqrt{m}\phi^{-\nu/(3\nu-1)} = R^*\left(\frac{\phi^*}{\phi}\right)^{\nu/(3\nu-1)} \tag{13}$$

The crossover length decreases as the power $\nu/(3\nu - 1) \cong 0.77$ of concentration (since $\nu = 0.59$). Note that the crossover length R_s decreases with concentration ϕ faster than the size R of micelles and therefore $R_s \ll R$ far above the overlap concentration (for $\phi \gg \phi^*$).

The high osmotic pressure causes the monomer distribution to be nearly uniform everywhere except in small regions close to the cores: $\phi(r) \simeq \phi$ for $R_s < r < R$. The soluble fragments are less stretched at $\phi \gg \phi^*$ (except for their small inner parts), hence, their elastic energy decreases with concentration. On the contrary, the osmotic free energy increases with concentration. The osmotic free energy density, Π, outside the small inner regions is proportional to the number density of concentration blobs[18]

$$\frac{\Pi}{k_BT} \approx \frac{\phi}{g} \approx \phi^{3\nu/(3\nu-1)} \simeq \phi^{2.3} \tag{14}$$

where the number of monomers per concentration blob is

$$g \approx \phi^{-1/(3\nu-1)} \simeq \phi^{-1.3} \tag{15}$$

Hence, osmotic energy is much higher than elastic energy at $\phi \gg \phi^*$. As a result, the system tends to keep the local monomer density constant (close to the average value ϕ) during structural transformations in order to avoid high osmotic energy penalty.

2.3. Elastic Free Energy. Let us consider the outer part of a micellar corona, i.e., the region $R/2 \lesssim r < R$. Elastic free energy per l-fragment (loop or bridge) can be written in terms of the ratio of its size R to the size R_l it would have at the same concentration if it were not attached to the core.[19]

$$F_{el} \approx k_BT\left(\frac{R}{R_l}\right)^2 \tag{16}$$

The size of a free l-fragment (unconnected to the core) in a semidilute solution at concentration ϕ is

$$R_l \approx \xi\left(\frac{l}{g}\right)^{1/2} \approx bl^{1/2}\phi^{-(\nu-1/2)/(3\nu-1)} \simeq bl^{1/2}\phi^{-0.12} \tag{17}$$

where $\xi \approx bg^\nu$ is the static correlation length (see eq 2) and the number of monomers, g, in a correlation blob decreases with concentration as shown in eq 15. Introducing the *elastic blob* g_{el} (elastic energy is k_BT per this blob), we can write the elastic free energy in terms of the number of elastic blobs per arm.

$$F_{el} \approx k_BT\frac{l}{g_{el}} \tag{18}$$

Combining two expressions for the elastic energy (eqs 16 and 18), we determine the number of monomers in an elastic blob

$$g_{el} \approx \frac{lR_l^2}{R^2} \approx \frac{l^{4/3}}{m^{2/3}}\phi^{1/[3(3\nu-1)]} \simeq \frac{l^{4/3}}{m^{2/3}}\phi^{0.43} \tag{19}$$

where eqs 12 and 17 were used. The ratio of the number of monomers in an elastic and concentration (osmotic) blobs can be estimated from eqs 9, 15, and 19.

$$\frac{g_{el}}{g} \approx \left(\frac{l}{\sqrt{m}}\right)^{4/3}\phi^{4/[3(3\nu-1)]} \approx \left(\frac{\phi}{\phi^*}\right)^{4/[3(3\nu-1)]} \simeq \left(\frac{\phi}{\phi^*}\right)^{1.7} \tag{20}$$

Hence, elastic blobs are always larger than osmotic blobs ($g_{el} > g$) above the overlap concentration of micelles (for $\phi > \phi^*$). This implies that the elongation of l-fragments (in the outer corona parts) does not significantly affect the structure at the osmotic blob scale. Yet loops and bridges are stretched ($R > R_l$ and $F_{el} > k_BT$) as long as there is more than one elastic blob per arm ($g_{el} < l$). The number of monomers in an elastic blob (eq 19) can be rewritten as

$$g_{el} \approx l\left(\frac{\phi}{\tilde{\phi}}\right)^{1/[3(3\nu-1)]} \simeq l\left(\frac{\phi}{\tilde{\phi}}\right)^{0.43} \tag{21}$$

where the crossover concentration is

$$\tilde{\phi} \approx \left(\frac{m^2}{l}\right)^{3\nu-1} \simeq \left(\frac{m^2}{l}\right)^{0.77} \tag{22}$$

At this crossover concentration, l-strands become undeformed $R(\tilde{\phi}) \approx R_l(\tilde{\phi})$, while they are stretched at lower concentrations $\phi < \tilde{\phi}$. This crossover concentration is much higher than overlap concentration of micelles

$$\frac{\tilde{\phi}}{\phi^*} \approx m^{3(3\nu-1)/2} \gg 1 \tag{23}$$

The total elastic energy in the outer corona part of a micelle is the elastic energy, F_{el}, for each of its l-strands times the number, m, of strands per micelle (eqs 18 and 21).

$$\mathcal{F}_{el} \approx mF_{el} \approx k_B T m \frac{l}{g_{el}} \approx k_B T m \left(\frac{\tilde{\phi}}{\phi}\right)^{1/[3(3\nu-1)]} \tag{24}$$

This elastic energy decreases with concentration as $\mathcal{F}_{el} \approx k_B T m(\tilde{\phi}/\phi)^{0.43}$ for $\nu \cong 0.59$.

2.4. Number of Bridges. A micellar corona consists of $m - \mathcal{N}$ loops and $2\mathcal{N}$ bridges connecting the micelle (flower) to its neighbors. At $\phi \sim \phi^*$ the fraction z of bridges is small ($z = \mathcal{N}/m \ll 1$), increasing slowly with concentration and saturating at $\tilde{\phi}$.[9]

$$\mathcal{N} \approx \begin{cases} m^{5/6}(\phi/\phi^*)^{1/[9(3\nu-1)]} = m(\phi/\tilde{\phi})^{1/[9(3\nu-1)]} & \phi^* < \phi < \tilde{\phi} \\ m & \phi > \tilde{\phi} \end{cases} \tag{25}$$

In the micellar concentration range, $\phi^* < \phi < \tilde{\phi}$, the number of bridges increases as power 0.14 of concentration, $\mathcal{N} \sim \phi^{0.14}$. At $\phi < \tilde{\phi}$, both loops and bridges are strongly stretched: their actual length $L_b \approx R$ is much larger than their "intrinsic" size R_l. Hence, the bridges are connecting the neighboring micelles in this regime ($\phi < \tilde{\phi}$). At higher concentrations, $\phi > \tilde{\phi}$, the bridges are nearly undeformed and they are typically connecting distant aggregates (rather than the nearest neighbors): the bridge size $L_b \approx R_l$ is larger than the interaggregate distance, R, in this regime. For concentrations $\phi > \tilde{\phi}$, the flowers lose most of their "petals" and the number of bridges per aggregate is close to m, while the fraction of loops is small. Thus, the size of a bridge or a loop is (eqs 12 and 17)

$$L_b \approx \begin{cases} R \approx b\left(\frac{lm}{\phi}\right)^{1/3} & \text{for } \phi^* < \phi < \tilde{\phi} \\ R_l \approx bl^{1/2}\phi^{-(\nu-1/2)/(3\nu-1)} & \text{for } \phi > \tilde{\phi} \end{cases} \tag{26}$$

2.5. Interaction between Micelles. Let us first consider the regime, $\phi^* < \phi < \tilde{\phi}$. Suppose a micellar core is displaced by a distance $\sim R$ from its equilibrium position and gets closer to one of its neighboring aggregates. The resultant free energy increase, $\Delta\mathcal{F}$, incorporates the elastic free energy increment, $\Delta\mathcal{F}_{el}$, and the osmotic increment, $\Delta\mathcal{F}_{osm}$. However, if the monomer concentration is kept nearly uniform (everywhere except in the regions near the cores, as discussed above), then the osmotic free energy does not change, hence $\Delta\mathcal{F} \approx \Delta\mathcal{F}_{el}$. Further, we may assume that it is the chain fragments in the softer outer parts of the coronas that are considerably deformed as a result of the displacement. Hence, the deformation energy must be on the order of the elastic energy of the outer corona part (eq 24)

$$\Delta\mathcal{F} \approx \mathcal{F}_{el} \approx k_B T m \left(\frac{\tilde{\phi}}{\phi}\right)^{1/[3(3\nu-1)]} \tag{27}$$

where $\tilde{\phi}$ is the crossover concentration defined in eq 22. This deformation energy decreases with concentration as $\Delta\mathcal{F} \sim \phi^{-0.43}$. The decrease of deformation energy, $\Delta\mathcal{F}$, with concentration is the source of many unusual dynamical properties of these associating polymers.

Let us turn to the higher concentration regime, $\phi > \tilde{\phi}$. Here the typical size of both loops and bridges is on the order of $R_l \gg R$ (see eq 26), so that bridges connecting different pairs of micelles are strongly overlapping. The bridges are weakly stretched both globally and locally on the length scale, R. Interaction between block-copolymer micelles in this regime was considered in ref 20. The result is directly applicable to the present system: the energy of interaction between two (neighboring) micelles depends on the distance d between their cores according to the $1/d$ law

$$\mathcal{F}_{int} \approx k_B T \frac{A}{d}, \text{ for } R_s \ll d \ll R_l \tag{28}$$

where the coefficient A is

$$A = \frac{6lv(2m)^2}{8\pi\phi R_l^2} \approx bm^2\phi^{-\nu/(3\nu-1)} \tag{29}$$

The deformation energy, $\Delta\mathcal{F}$, is then equal to the interaction energy increment due to a displacement of the micellar core by the distance, d, of the order of intermicellar spacing, R (eq 12).

$$\Delta\mathcal{F} \approx k_B T \frac{A}{R} \approx k_B T \frac{m^{5/3}}{l^{1/3}}\phi^{-1/[3(3\nu-1)]} \tag{30}$$

Note that the right-hand sides of eqs 27 and 30 coincide, i.e., the deformation energy has the same scaling form in both regimes.

2.6. Elastic Modulus Due to Micelles. A shear deformation (with strain $\gamma \approx 1$) would result in the elastic energy increment of $\Delta\mathcal{F}$ per micelle. Hence, the shear elastic modulus of the reversible gel is

$$G_m \approx \frac{\Delta\mathcal{F}}{R^3} \approx \frac{k_B T}{b^3}\frac{m^{2/3}}{l^{4/3}}\phi^{1-1/[3(3\nu-1)]} \tag{31}$$

The modulus increases as a power of concentration $G \sim \phi^{0.57}$ because $\nu \cong 0.59$.

This equation is valid for an unentangled micellar phase above the overlap concentration of micelles (for $\phi > \phi^*$). If the system is entangled ($N > N_e(\phi)$), eq 31 is applicable at intermediate time scales: longer than the disentanglement time but shorter than the reversible gel structure relaxation time.

2.7. Chain Dimensions. Each associating polymer chain can be considered as a sequence of loops and bridges. The fraction of bridges is $z = \mathcal{N}/m$ and the mean number of bridges per chain is $n = fz$. We will assume that this number is large

$$n = fz \gg 1 \tag{32}$$

Disregarding loops, we may consider an associating macromolecule as a chain of $n = fz$ random steps (bridges) of length, L_b (eq 26). Correlation between the step directions can be neglected as the concentration blob size is always much smaller than the bridge size L_b. Hence, the chain size $R_N \approx n^{1/2}L_b \approx (f\mathcal{N}/m)^{1/2}L_b$. Recall the size of a bridge (eq 26) is $L_b \approx 2R$ (intermicellar distance) for $\phi^* < \phi < \tilde{\phi}$ and $L_b \approx R_l$ (unperturbed size) for $\phi > \tilde{\phi}$. Using eqs 17 and 25 we get

$$R_N \approx bN^{1/2}\phi^{-(\nu-1/2)/(3\nu-1)}\begin{cases}\left(\frac{\tilde{\phi}}{\phi}\right)^{1/[9(3\nu-1)]} & \phi^* < \phi < \tilde{\phi} \\ 1 & \phi > \tilde{\phi}\end{cases} \quad (33)$$

Note that the size of the chain decreases with concentration in the micellar regime ($\phi^* < \phi < \tilde{\phi}$) ($R_N \sim \phi^{-0.26}$), even though the number of bridges per chain increases in this regime. The reason for this decrease of the chain size is that the decrease in the size of the bridge (eq 26) dominates over the slow increase in the number of bridges (eq 25). At higher concentrations ($\phi > \tilde{\phi}$), decrease of polymer size is weaker $R_N \sim \phi^{-0.12}$ and is entirely due to the decrease of the size of bridges (eq 26).

3. Sticker and Chain Dynamics

3.1. Dissociation of Stickers. The elementary event in the dynamics of associating polymers is a sticker dissociation from an aggregate and its association with another aggregate. In the case of pairwise association ($m = 2$), we showed[7,8] that a sticker tends to return many times to its previous partner before it forms a new bond (in the strong association regime, $\epsilon \gg 1$). The case of large aggregates ($m \gg 1$), considered in the present work, is different. We do not expect a unique stable aggregation number m, but rather it is likely that aggregation numbers are distributed around a mean value, so that micelles with m and $m \pm 1$ stickers are nearly equally probable. Sticker dissociation from an m-aggregate and its attachment to a neighboring m -aggregate results in a formation of two micellar cores with $m - 1$ and $m + 1$ stickers, correspondingly. The net free energy variation, ΔE, due to this process is $\Delta E = E(m + 1) + E(m - 1) - 2E(m)$, where $E = E(m)$ is the energy of a micellar core with m stickers. In the present paper, we assume that this process is *not* suppressed thermodynamically, i.e., $\Delta E < k_BT$. The energy change upon sticker rearrangement ΔE can be approximated as $\Delta E \simeq \partial^2 E/\partial m^2$. The energy $E(m)$ of a micelle contains contribution from the bulk of the core $E_b m$ linear in aggregation number m and contribution $E_s m^{2/3}$ from the core surface energy, hence $E(m) \approx E_b m + E_s m^{2/3}$. Note that the energy difference before and after sticker association is controlled by the change in the surface energy of the core $\epsilon k_BT = E(1) + E(m - 1) - E(m) \approx E_s$. Therefore, the surface energy of a micellar core is $E(m) - E_b m \approx \epsilon k_BT m^{2/3}$ and the free energy variation $\Delta E \simeq \partial^2 E/\partial m^2 \approx \epsilon k_BT m^{-4/3}$. The condition $\Delta E < k_BT$ reduces to

$$\epsilon < m^{4/3} \quad (34)$$

With this condition we may entirely neglect the renormalization of the reversible bond lifetime, τ_b, considered in refs. 7 and 8. The bond lifetime, therefore, has its bare value

$$\tau_b = \tau_0 \exp(\epsilon + \epsilon_a) = \tau_0 \exp \epsilon_{tot} \quad (35)$$

where τ_0 is the microscopic time characterizing sticker diffusion and $\epsilon_{tot}k_BT$ is the activation energy for a sticker dissociation. The total activation energy incorporates the net dissociation energy, ϵk_BT, and the additional energy barrier, $\epsilon_a k_BT$.

$$\epsilon_{tot} = \epsilon + \epsilon_a \quad (36)$$

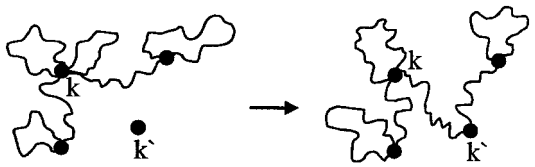

Figure 3. Elementary step of the Sticky Rouse motion. A sticker dissociates from the core of one micelle (k) and associates with the core of another micelle (k'). Only a part of one chain is shown for clarity. Cores of micelles are represented by black circles.

Both energies are related to the micellar core structure. Recall that we have assumed that $\epsilon > m^{1/2}$ (eq 11) and therefore the dissociation energy is limited to the interval $m^{1/2} < \epsilon < m^{4/3}$.

3.2. Chain Diffusion: Rouse Dynamics. Let us consider the dynamics of associating polymer chains in the micellar phase ($\phi > \phi^*$) assuming first that the chains are unentangled. Once a sticker is dissociated, it will (most probably) be driven away from its parent core by the tension of strongly stretched l-fragments attached to it. It will wiggle in space between the flower micelles for some time before approaching the core of a neighboring micelle, thus forming a new bond. Obviously, the wiggling time is much shorter than the bond lifetime, τ_b. Hence, τ_b defines the sticker hopping time.

Let us estimate the Rouse conformational relaxation time, τ_R, of a chain. We may consider micellar cores as lattice sites and represent the chain conformation as a walk on this lattice, i.e., by the sequence $\{r_1, r_2, ..r_n\}$ of lattice sites visited by the chain. Each core is typically visited repeatedly, with ν_k guest stickers of the chain per core r_k, $\langle \nu_k \rangle = 1/z = m/\mathcal{N}$, so that the number of visited cores $n \simeq fz$. Hence, the chain can be viewed as a sequence of cores connected by bridges. Every two consecutive bridges are connecting core r_k to its two distinct neighbors r_{k-1} and r_{k+1}; in the case when $r_{k-1} = r_{k+1}$, the core r_k is not counted and all of its stickers are attributed to the neighboring core r_{k-1}. The number of "guest" stickers ν_k in the kth core may change by elementary steps, as shown in Figure 3. The time of each step ($\nu_k \rightarrow \nu_k \pm 1$) is of the order of the sticker hopping time, τ_b. To abandon a particular core the chain has to decrease the number of guest stickers from $\nu \sim 1/z$ to 0, the corresponding time

$$\tau_1 \approx \tau_b \nu^2 \approx \frac{\tau_b}{z^2} \quad (37)$$

The number of guest stickers per micelle, $\nu(t)$, changes by a random process, hence time τ_1 depends on the square of the number of guest stickers, ν. The time, τ_1, is the segment relaxation time for the coarse chain $\{r_1, r_2, ..r_n\}$. The longest Rouse relaxation time of the chain is thus

$$\tau_R \approx \tau_1 n^2 \approx \tau_b f^2 \quad (38)$$

where we used eq 32 relating the number of micelles per chain n to the fraction of bridges z. Note that it has the form of the Rouse time of a chain with f stickers with lifetime τ_b per sticker and does not depend on the number n of micelles per chain nor on the number ν of guest stickers per micelle.

3.3. Chain Diffusion: Entangled Chains. We now consider the implications of the fact that chain sections cannot intersect each other in the process of chain

motion. A standard way to describe these topological constraints is to assume a confining tube restricting the dynamics of each polymer chain (the de Gennes-Doi-Edwards reptation model). The confinement length scale is the tube diameter, a_e, which is equal to the size of the topological blob, a chain fragment consisting of N_e monomers (N_e is often referred to as the number of monomers per *entanglement*). The topological blob is always larger than the concentration blob

$$N_e = N_{e0}g \approx N_{e0}\phi^{-1/(3\nu-1)} \simeq N_{e0}\phi^{-1.3} \tag{39}$$

where N_{e0} is a large parameter (normally $N_{e0} \sim 20 \div 100$) corresponding to the number of monomers per entanglement in a melt. A topological blob in a semidilute solution is then a Gaussian chain of N_{e0} concentration blobs, hence its size

$$a_e \approx {N_{e0}}^{1/2}\xi \approx b{N_{e0}}^{1/2}\phi^{-\nu/(3\nu-1)} \simeq b{N_{e0}}^{1/2}\phi^{-0.77} \tag{40}$$

In the micellar phase the spacer fragments (l-fragments) are stretched (in the regime $\phi^* < \phi < \tilde{\phi}$), hence, its 'topological' structure is possibly different from that in a semidilute solution at the same concentration ϕ. The local chain stretch may affect N_e and may also result in anisotropic tubes. We do not consider these complications here and simply neglect the effect of the local chain stretching on entanglements. This approximation should be perfectly valid if topological blobs are weakly stretched, i.e., $N_e(\phi) < g_{el}$. This condition is equivalent to $\phi > \phi^* {N_{e0}}^{3(3\nu-1)/4}$.

We consider two regimes of entanglements: (i) weakly entangled regime with entangled chains, but unentangled l-spacers and (ii) strongly entangled regime with entangled l-spacers.

3.3.1. Weakly Entangled Regime ($l < N_e(\phi) < N$). Chains are entangled in this regime, but the l-spacers are not. Weakly entangled regime corresponds to the concentration range $\phi_e^* < \phi < \phi_e$, where the onset of entanglement for the whole chain ($N_e(\phi_e^*) = N$) occurs at concentration (eq 39)

$$\phi_e^* \approx \left(\frac{N_{e0}}{N}\right)^{3\nu-1} \tag{41}$$

while the spacers between stickers entangle ($N_e(\phi_e) = l$) at concentration

$$\phi_e \approx \left(\frac{N_{e0}}{l}\right)^{3\nu-1} \tag{42}$$

In the weakly entangled regime the tube diameter is larger than the segment (spacer) size, and so the segment relaxation time (τ_1) is not affected by entanglements. The chain conformation relaxation time is then the reptation time with the relevant (curvilinear) friction constant being defined by τ_1. Hence, the well-known general relation between the reptation time, τ_{rept}, and the Rouse time, τ_R,[21] is applicable.

$$\tau_{rept} \approx \tau_R \frac{N}{N_e(\phi)} \approx \tau_b f^3 \frac{l}{N_e(\phi)} \tag{43}$$

3.3.2. Strongly Entangled Regime ($N_e(\phi) < l$). The strongly entangled regime corresponds to concentrations higher than entanglement onset of l-spacers between stickers ($\phi > \phi_e$). In this regime, l-spacers are entangled and *entanglements do affect sticker hops* as shown in Figure 4.

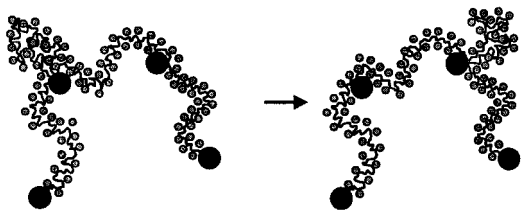

Figure 4. Elementary step of reptation in strongly entangled regime by transport of unentangled loops. Large circles represent cores of micelles. Small circles represent entanglement constraints imposed by surrounding chains.

Transport by Unentangled Loops. During a hop, one l-loop and an adjacent bridge are transformed into a bridge and a loop, respectively (Figure 4). However, this process is arrested if the initial l-loop is entangled. Hence, only stickers with an unentangled adjacent loop can hop. The fraction of these stickers is equal to the probability that a loop is unentangled, $p_e = e^{-Fe/k_BT}$, where the corresponding free energy is proportional to the number of entanglements per l-stand

$$F_e \approx k_BT\frac{l}{N_e(\phi)} \approx k_BT\frac{l}{N_{e0}}\phi^{1/(3\nu-1)} \approx k_BT\left(\frac{\phi}{\phi_e}\right)^{1/(3\nu-1)} \tag{44}$$

This free energy increases with concentration as $F_e/(k_BT) \sim (\phi/\phi_e)^{1.3}$ for $\nu \cong 0.59$. Note that as a result of a sticker hop, an unentangled loop 'jumps' from a micelle to a neighboring one (Figure 4). Therefore, unentangled loops can be considered as mobile kinks propagating (diffusing) along the chain. The reptation time is inversely proportional to the number of these kinks, i.e.,

$$\tau_{rept} \approx \frac{\tau_b f^3}{p_e} \approx \tau_b f^3 \exp\left(\frac{F_e}{k_BT}\right) \approx \tau_b f^3 \exp\left[\left(\frac{\phi}{\phi_e}\right)^{1/(3\nu-1)}\right] \tag{45}$$

Hence, the chain relaxation time increases exponentially with 1.3 power of concentration in this regime.

Collective Tube Leakage. The dynamical mechanism considered above accounts for just one reptation channel due to diffusion of kinks. Another possible channel that is relevant at high concentrations is described below. To simplify the argument we assume that

$$m^2 > N_{e0} \tag{46}$$

i.e., $\phi_e < \tilde{\phi}$ and the system is already strongly entangled at $\tilde{\phi}$.

Consider a sticker attached to the core k and connected by bridging l-fragments with cores (micelles) $k - 1$ and $k + 1$. Now suppose that the sticker dissociates from the core k and (being still bridged to cores $k - 1$ and $k + 1$) associates with a different core k'. This process when repeated by many stickers will result in the chain reptation. However it requires that a new partner (core k') is accessible. Typically, the sticker (when bridged to cores $k - 1$ and $k + 1$) can explore a tube section of length $\Delta L \approx R_l$ with the corresponding tube volume $\Delta V \approx \Delta L a_e^2$ and the mean number of micellar cores in this volume $\Delta n \approx \Delta V\phi/(lmb^3)$, where $\phi/(lmb^3)$ is the number density of micelles. The average

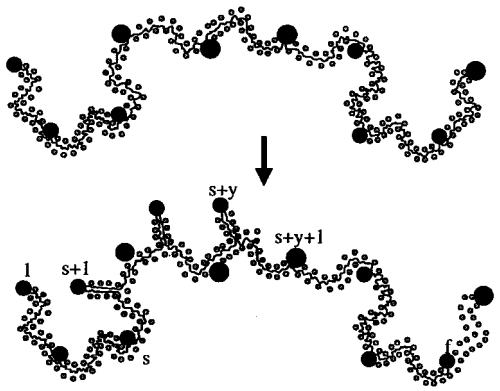

Figure 5. Collective tube leakage ($f = 10, y = 3, s = 3$). Large circles represent cores of micelles. Only one chain is shown for clarity. Small circles represent entanglement constraints imposed on the chain by surrounding chains. Labels correspond to the stickers on the chain.

number of micelles in the sticker fluctuation volume ΔV

$$\Delta n \approx R_l {a_e}^2 \frac{\phi}{lmb^3} \approx \frac{N_{e0}}{m^2}\left(\frac{\phi}{\tilde{\phi}}\right)^{-1/[2(3\nu-1)]} \tag{47}$$

is small ($\Delta n < 1$) at high concentrations (say, at $\phi > \tilde{\phi}$) with condition 46. Therefore the sticker has to leave its tube by double-folding x entanglement strands (Figure 5) in order to reach the core of the neighboring micelle distance R away,[22] where

$$x = \frac{R}{a_e} \approx \frac{b}{a_e}\left(\frac{lm}{\phi}\right)^{1/3} \approx \frac{(lm)^{1/3}}{{N_{e0}}^{1/2}}\phi^{1/[3(3\nu-1)]} \approx \sqrt{\frac{m^2}{N_{e0}}}\left(\frac{\phi}{\tilde{\phi}}\right)^{1/[3(3\nu-1)]} \tag{48}$$

is large ($x \gg 1$) at high concentrations.

This unfavorable "leaked out" conformation raises the free energy of the chain by k_BTx. Naively, one may expect that in order for a chain to reptate, most of its stickers have to abandon their home micelles and to find new hosts by leakage. The corresponding activation energy is the total number of stickers, f, times the energy barrier per sticker, k_BTx. To avoid this huge barrier, most of the stickers must stay in their original homes or in the homes of their neighbors. For example, stickers from 1 to s stay in their home micelles, stickers from $s + 1$ to $s + y$ are leaked out of the tube forming a collective kink, stickers from $s + y + 1$ to f occupy home micelles of their nearest-left neighbors. The collective kink is a chain section of y stickers. This kink section occupies a tube fragment that was originally occupied by $y - 1$ stickers. As the kink moves from head to tail of the chain (as s changes from f to 1), the chain makes one reptation step. This kink contains yl monomers and occupies $(y - 1)l/N_e$ entanglement sections of the original tube and xy entanglement sections through which the kink leaks out of the original tube in the form of y double-folded unentangled loops.

The relative deformation (extension) of the kink along the tube is $\epsilon = a_e[(y - 1)l/N_e + xy]/L_y - 1$, where $L_y = a_e yl/N_e$ is the equilibrium tube length of the kink containing yl monomers. Hence, the elastic energy of the kink is

$${F_e}^* \sim k_BT\frac{yl}{N_e}\epsilon^2 \sim k_BT\frac{l}{yN_e}\left(1 - xy\frac{N_e}{l}\right)^2 \sim k_BT\frac{l}{yN_e} \tag{49}$$

In the last '$\sim$' we assumed that $xy < l/N_e$ (to be verified below). Adding the free energy of double folding, k_BTxy, to ${F_e}^*$ we get the total kink activation energy

$$F^* = {F_e}^* + k_BTxy \sim k_BT\left(\frac{l}{yN_e(\phi)} + xy\right) \tag{50}$$

Minimizing the kink activation energy (eq 50) with respect to the number of stickers y in it leads to

$$y \approx \sqrt{\frac{l}{xN_e(\phi)}} \tag{51}$$

and the free energy cost F^* of the optimal kink is

$$F^* \approx k_BT\sqrt{\frac{lx}{N_e(\phi)}} \approx k_BT\frac{l^{2/3}m^{1/6}}{{N_{e0}}^{3/4}}\phi^{2/[3(3\nu-1)]} \approx k_BT\left(\frac{m^2}{N_{e0}}\right)^{3/4}\left(\frac{\phi}{\tilde{\phi}}\right)^{2/[3(3\nu-1)]} \tag{52}$$

This free energy cost is lower than that for transport by unentangled loops ($F_e \approx k_BTl/N_e(\phi)$) for concentrations higher than

$$\phi_{kink} \approx \left(\frac{{N_{e0}}^{3/4}m^{1/2}}{l}\right)^{3\nu-1} \approx \phi_e\left(\frac{m^2}{N_{e0}}\right)^{(3\nu-1)/4} \approx \tilde{\phi}\left(\frac{N_{e0}}{m^2}\right)^{3(3\nu-1)/4} \tag{53}$$

where the entanglement concentration for l-strands ϕ_e is given in eq 42 and the crossover concentration $\tilde{\phi}$ is defined in eq 22. Since it was assumed that $m^2 > N_{e0}$ (see relation 46), one concludes that

$$\phi_e < \phi_{kink} < \tilde{\phi} \tag{54}$$

The assumed condition $xy < l/N_e$ simply follows from the condition $F^* < F_e$ that ensures that the collective kink dynamics is relevant at all.

The transport by unentangled loops dominates in the concentration regime $\phi_e < \phi < \phi_{kink}$, while the transport by collective kinks is the dominant mechanism at higher concentrations $\phi > \phi_{kink}$. The free energy of the optimal collective kink (eq 52) can be written as

$$F^* \approx k_BT\left(\frac{\phi_{kink}}{\phi_e}\right)^{1/(3\nu-1)}\left(\frac{\phi}{\phi_{kink}}\right)^{2/[3(3\nu-1)]} \tag{55}$$

The chain relaxation time in the collective tube leakage mode also increases exponentially with concentration

$$\tau_{rept} \approx \tau_b f^3 \exp\left(\frac{F^*}{k_BT}\right) \tag{56}$$

but with a weaker power law in the exponent

$$\ln(\tau_{rept}) \sim \frac{F^*}{k_BT} \sim \phi^{2/[3(3\nu-1)]} \sim \phi^{0.87} \text{ for } \phi > \phi_{kink} \tag{57}$$

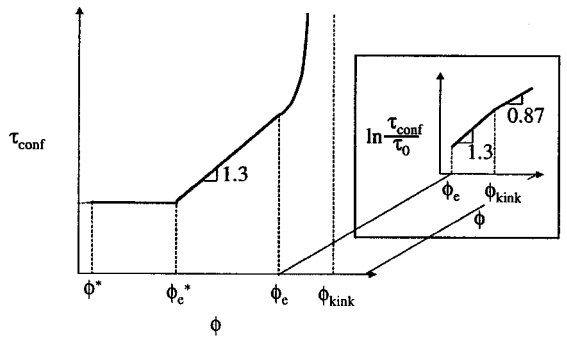

Figure 6. Concentration dependence of conformational relaxation time of a chain τ_{conf}. Logarithmic scale. Inset: Logarithm of chain reptation time $\ln(\tau_{conf}/\tau_0)$ for strongly entangled regime. Logarithmic scales.

instead of

$$\ln(\tau_{rept}) \sim \frac{F_{el}}{k_B T} \sim \phi^{1/(3\nu-1)} \sim \phi^{1.3} \text{ for } \phi_e < \phi < \phi_{kink} \tag{58}$$

for the transport by unentangled loops.

The chain conformation relaxation time τ_{conf} in the micellar gel can be defined as Rouse time $\tau_{conf} = \tau_R$ for unentangled chains (eq 38) or as reptation time $\tau_{conf} = \tau_{rept}$ for entangled chains (eqs 43, 45, or 56 depending on the concentration regime). Combining eqs 38, 43, 45, and 56 we can obtain expressions for the logarithm of chain conformational relaxation time, $\ln(\tau_{conf})$, in different concentration regimes.

$$\ln\left(\frac{\tau_{conf}}{\tau_0}\right) \approx \begin{cases} \epsilon_{tot} + 2\ln f & \text{for } \phi^* < \phi < \phi^*_e \\ \epsilon_{tot} + 3\ln f + \dfrac{1}{3\nu-1}\ln\left(\dfrac{\phi}{\phi_e}\right) & \text{for } \phi^*_e < \phi < \phi_e \\ \epsilon_{tot} + 3\ln f + \left(\dfrac{\phi}{\phi_e}\right)^{1/(3\nu-1)} & \text{for } \phi_e < \phi < \phi_{kink} \\ \epsilon_{tot} + 3\ln f + \left(\dfrac{\phi_{kink}}{\phi_e}\right)^{1/(3\nu-1)}\left(\dfrac{\phi}{\phi_{kink}}\right)^{2/(3\nu-1)} & \text{for } \phi > \phi_{kink} \end{cases} \tag{59}$$

The concentration dependence of polymer conformation relaxation time, τ_{conf}, is sketched in Figure 6 . The chain conformational relaxation time is concentration independent in unentangled regime ($\phi^* < \phi < \phi_e^*$) and increases as 1.3 power of concentration in weakly entangled regime ($\phi_e^* < \phi < \phi_e$). In strongly entangled regimes τ_{conf} increases exponentially with powers of concentration (as plotted in the insert in Figure 6).

4. Dynamics of Micelles

4.1. The Hopping Time. We consider the micellar gel as a closely packed amorphous system of micelles (see Figure 2). In other words, we assume a short-range liquidlike arrangement of micelles, with individual micelles hopping from one position to another (Figure 7), hence, diffusing.[23] This process requires a high activation energy,[9] which is in part due to the deformation of the hopping micelle and its neighbors. The micellar hopping time τ_h that corresponds to the terminal relaxation time of the system is then exponentially long. It is convenient to define this hopping time in terms of the *effective exponent*, E, using a simple definition $\tau_h = \tau_0 e^E$.

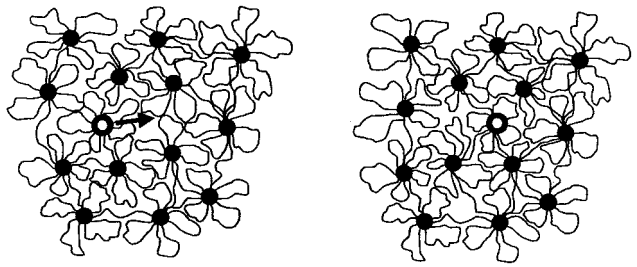

Figure 7. Hopping of a micelle denoted by a core with a white center.

$$E = \ln(\tau_h/\tau_0) \tag{60}$$

The corresponding deformation energy, $\Delta\mathcal{F}$, can be defined as the maximum deformation energy during the displacement of the micellar core from one cell into another, i.e., by a distance on the order of the intermicellar spacing. This deformation energy was calculated above, (eqs 27, 30)

$$\Delta\mathcal{F} \approx k_B T m\left(\frac{\tilde{\phi}}{\phi}\right)^{1/[3(3\nu-1)]} \tag{61}$$

and decreases with increasing concentration. *To hop into a new cell a micelle has to remove its bridges with the old neighbors and create new bridges. Also, all the entanglements with the old neighbors must be relaxed.* Hopping of a micelle can proceed via either of the two possible pathways.

Kinetic Pathway 1. One way to move a micelle is just to allow for all involved polymer chains to be relaxed at all stages of the core displacement. Hence the hopping time

$$\tau_{h1} \sim \tau_{conf} \exp\left(\frac{\Delta\mathcal{F}}{k_B T}\right) \tag{62}$$

where τ_{conf} is the chain conformation relaxation time in the micellar gel (eq 59). Here and below we ignore preexponential factors that show relatively weak concentration dependencies. The corresponding effective exponent is then (according to eq 60)

$$E_1 = \frac{\Delta\mathcal{F}}{k_B T} + \ln\left(\frac{\tau_{conf}}{\tau_0}\right) \tag{63}$$

We will see below that Kinetic Pathway 1 is dominant at higher concentrations (for $\phi > \tilde{\phi}$) and in some cases also at lower concentrations.

Kinetic Pathway 2. The Kinetic Pathway 1 may not be the optimal one if the conformational relaxation time of a chain τ_{conf} is too long. In this case, there is an alternative kinetic pathway described below. First, a micelle is prepared for a hop and nearly all of its old bridges are removed (transformed to loops). The corresponding free energy increase, F_b, is of the order of $k_B T$ times the equilibrium number of bridges per micelle

$$F_b \approx k_B T \mathcal{N} \tag{64}$$

Then, the micellar core moves into a new cell without dissociation of its stickers requiring an additional deformation energy cost, F_d. The net effective activation energy is then

$$F_a = F_b + F_d \tag{65}$$

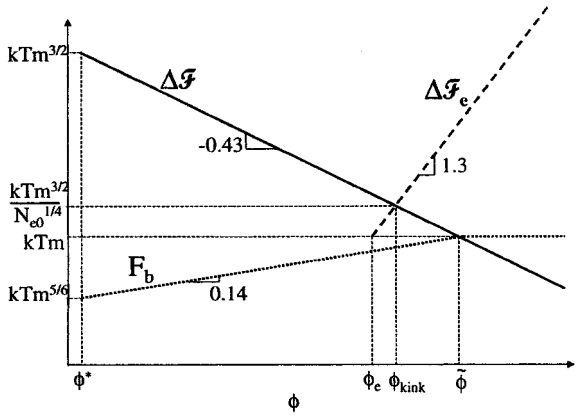

Figure 8. Concentration dependence of the three components of the activation energy, $F_a = F_b + \Delta\mathcal{F} + \Delta\mathcal{F}_e$, for the Kinetic Pathway 2. Logarithmic scales.

The deformation energy, F_d, consists of a phantom part, $\Delta\mathcal{F}$, and an entanglement part, $\Delta\mathcal{F}_e$. The phantom part, $\Delta\mathcal{F}$ (without an entanglement effect), was calculated above (see eqs 27, 30, or 61). The extra deformation energy, $\Delta\mathcal{F}_e$, due to entanglements is on the order of k_BT times the number of these entanglements per micelle (as the typical strain is ~1)

$$\Delta\mathcal{F}_e \approx k_BT\frac{ml}{N_e(\phi)} \approx mF_e \approx k_BTm\left(\frac{\phi}{\phi_e}\right)^{1/(3\nu-1)} \quad (66)$$

Hence, in the general case, $F_d = \Delta\mathcal{F} + \Delta\mathcal{F}_e$, and the activation energy is

$$F_a = F_b + F_d = F_b + \Delta\mathcal{F} + \Delta\mathcal{F}_e$$

$$\approx k_BTm\left(\left(\frac{\phi}{\tilde{\phi}}\right)^{1/[9(3\nu-1)]} + \left(\frac{\tilde{\phi}}{\phi}\right)^{1/[3(3\nu-1)]} + \left(\frac{\phi}{\phi_e}\right)^{1/(3\nu-1)}\right) \quad (67)$$

The three components of the activation energy, F_a, are sketched in Figure 8. For $N_{e0} < m^2$ the entanglement concentration for l-strands, ϕ_e, is lower than crossover concentration $\tilde{\phi}$ (see eqs 42 and 22) and therefore the activation energy F_a for the Kinetic Pathway 2 is dominated by the phantom part $\Delta\mathcal{F}$ of deformation energy (solid line in Figure 8) at lower concentrations ($\phi < \phi_{kink}$) and by the entanglement part $\Delta\mathcal{F}_e$ (dashed line in Figure 8) at higher concentrations ($\phi > \phi_{kink}$). The crossover between the phantom and entanglement parts of the deformation energy occurs at the same concentration ϕ_{kink} (eq 53) as the crossover between reptation by unentangled loops and collective tube leakage in the strongly entangled regime.

The contribution to the hopping time associated with the F_a-activation state is

$$\tau_a \approx \tau_m \exp\left(\frac{F_a}{k_BT}\right) \quad (68)$$

where

$$\tau_m \approx \frac{R^2}{D_m} \quad (69)$$

is the time of "free" (not restricted by entanglements) diffusion of a micelle by a distance of order R. It can be easily estimated from the distance between cores of micelles $R \approx b(lm/\phi)^{1/3}$ and the micellar Rouse−Zimm friction

$$\zeta_m \approx m\frac{l}{g}\xi\eta_s \approx \eta_s bml\phi^{(1-\nu)/(3\nu-1)} \quad (70)$$

where η_s is the solvent viscosity. The corresponding Rouse−Zimm diffusion coefficient of a micelle is

$$D_m = \frac{k_BT}{\zeta_m} \approx \frac{k_BT}{\eta_s bml}\phi^{-(1-\nu)/(3\nu-1)} \quad (71)$$

Hence, Rouse−Zimm time of a micelle is

$$\tau_m \approx \frac{R^2}{D_m} \approx \frac{\eta_s b^3}{k_BT}(ml)^{5/3}\phi^{-(9\nu-5)/[3(3\nu-1)]} \quad (72)$$

Taking into account that $\tau_0 \approx \eta_s b^3/(k_BT)$ and eq 22 we finally get Rouse−Zimm time of a micelle

$$\tau_m \approx \tau_0(ml)^{5/3}\phi^{-(1/3)-(9\nu-5)/[(3\nu-1)]} \approx \tau_0 l^{3\nu}m^{5-6\nu}\left(\frac{\tilde{\phi}}{\phi}\right)^{(9\nu-5)/[3(3\nu-1)]} \quad (73)$$

that has a very weak concentration dependence $\tau_m \sim \phi^{-0.13}$ and can be approximated by a constant.

Another possible bottleneck for hopping is the debridging process that is supposed to take place before the deformation of the hopping micelle and its neighborhood. The time required for elimination of one bridge is of the order of the reptation time τ_{conf}: one of the chain ends has to reptate down to the bridge to be eliminated. The total free energy penalty for debridging is $F_b \approx k_BT\mathcal{N}$, hence, the debridging time is

$$\tau_{db} \approx \tau_{conf}\exp\left(\frac{F_b}{k_BT}\right) \approx \tau_{conf}\exp(\mathcal{N}) \quad (74)$$

A step of the Kinetic Pathway 2 consists of two parts: the debridging part with duration τ_{db} and the hopping part of length τ_a. Therefore, the total hopping time associated with the Kinetic Pathway 2 is the sum of the durations of the two parts $\tau_{h2} \simeq \tau_a + \tau_{db}$ with the corresponding effective exponent dominated by the longest part of the process $E_2 = \ln(\tau_{h2}/\tau_0) \approx \max[\ln(\tau_a/\tau_0), \ln(\tau_{db}/\tau_0)]$, i.e.,

$$E_2 \approx \max\left[\frac{F_a}{k_BT} + \ln\frac{\tau_m}{\tau_0}, \frac{F_b}{k_BT} + \ln\frac{\tau_{conf}}{\tau_0}\right] \quad (75)$$

Both kinetic pathways do contribute to the hopping frequency and the resulting hopping rate of a micelle is the sum of the hopping rates of both kinetic pathways.

$$1/\tau_h = 1/\tau_{h1} + 1/\tau_{h2} \quad (76)$$

The fastest of the kinetic pathways determines the hopping time, τ_h. Hence, neglecting preexponential factors, we can approximate the effective exponent, E, of the micellar hopping process by the smaller of the effective exponents of the two kinetic pathways.

$$E = \min\{E_1, E_2\}$$
$$\approx \min\left\{\left(\frac{\Delta\mathscr{T}}{k_BT} + \ln\frac{\tau_{conf}}{\tau_0}\right), \max\left[\left(\frac{F_a}{k_BT} + \ln\frac{\tau_m}{\tau_0}\right), \left(\frac{F_b}{k_BT} + \ln\frac{\tau_{conf}}{\tau_0}\right)\right]\right\} \quad (77)$$

Here, the deformation energy of a micelle $\Delta\mathscr{T}$ is defined in eq 61, the activation energy, F_a, of Kinetic Pathway 2 is given by eq 67, and free energy cost for debridging is determined by eqs 64 and 25. The term $\ln(\tau_m/\tau_0)$ shows a weak (logarithmic) concentration dependence (eq 73). The conformation relaxation time τ_{conf} increases with concentration in entangled regimes (eq 59). The longest conformation relaxation time τ_{conf} is attained at $\phi \sim 1$ with $\ln(\tau_{conf}/\tau_0) \approx \epsilon_{tot} + m^{1/6}l^{2/3}/N_{e0}{}^{3/4}$.

The concentration dependence of terminal relaxation time $\tau_h = \tau_0 e^E$ is essentially determined by the value of the activation energy, ϵ_{tot}, for sticker dissociation (eq 36). Whether debridging or hopping processes control the Kinetic Pathway 2 (eq 75) depends on the relative value of ϵ_{tot} dominating debridging and $F_d/(k_BT)$ dominating hopping (eq 67). The largest deformation energy, F_d, of a micelle in the concentration interval $\phi^* < \phi < \tilde{\phi}$ (Figure 8) is either due to its phantom part

$$\Delta\mathscr{T}(\phi^*) \approx k_BTm(\tilde{\phi}/\phi^*)^{1/[3(3\nu-1)]} \approx k_BTm^{3/2} \quad (78)$$

if $N_{e0} > m^{3/2}$ or is due to its entanglement part

$$\Delta\mathscr{T}_e(\tilde{\phi}) \approx k_BTm(\tilde{\phi}/\phi_e)^{1/(3\nu-1)} \approx k_BT\frac{m^3}{N_{e0}} \quad (79)$$

if $N_{e0} < m^{3/2}$.

Case A. For $\epsilon_{tot} \gtrsim \max(m^{3/2}, m^3/N_{e0})$ the debridging process dominates the Kinetic Pathway 2 in the concentration range $\phi^* < \phi < \phi_A$, while the hopping process dominates at higher concentrations ($\phi > \phi_A$) with the effective exponent of this Pathway

$$E_2 \approx \begin{cases} \dfrac{F_b}{k_BT} + \ln\dfrac{\tau_{conf}}{\tau_0} & \text{for } \phi^* < \phi < \phi_A \\ \dfrac{\Delta\mathscr{T}_e + \Delta\mathscr{T} + F_b}{k_BT} + \ln\dfrac{\tau_m}{\tau_0} & \text{for } \phi > \phi_A \end{cases} \quad (80)$$

The crossover concentration between the two regimes

$$\phi_A \approx \phi_e\left(\frac{\epsilon_{tot}}{m}\right)^{3\nu-1} \approx \tilde{\phi}\left(\frac{\epsilon_{tot}N_{e0}}{m^3}\right)^{3\nu-1} \quad (81)$$

is the concentration at which the entanglement part of the deformation energy $\Delta\mathscr{T}_e/k_BT \approx m(\phi/\phi_e)^{1/(3\nu-1)}$ is on the order of ϵ_{tot}. Note that in Case A, $\epsilon_{tot} > m^3/N_{e0}$ and the crossover concentration $\phi_A > \tilde{\phi}$.

The effective exponent, E, for micelle hopping (eq 77) is determined in the concentration range $\phi^* < \phi < \phi_A$ by the smallest of the micelle deformation free energy, $\Delta\mathscr{T}$ (Kinetic Pathway 1), and debridging free energy, F_b (Kinetic Pathway 2). Debridging free energy $F_b \approx k_BTm(\phi/\tilde{\phi})^{1/[9(3\nu-1)]}$ is smaller than micellar deformation free energy $\Delta\mathscr{T} \approx k_BTm(\tilde{\phi}/\phi)^{1/[3(3\nu-1)]}$ at lower concentrations $\phi < \tilde{\phi}$, while micellar deformation free energy is smaller in the concentrations regime of overlapping micelles $\phi > \tilde{\phi}$.

$$E \approx \begin{cases} \dfrac{F_b}{k_BT} + \ln\dfrac{\tau_{conf}}{\tau_0} & \text{for } \phi < \tilde{\phi} \\ \dfrac{\Delta\mathscr{T}}{k_BT} + \ln\dfrac{\tau_{conf}}{\tau_0} & \text{for } \phi > \tilde{\phi} \end{cases} \quad (82)$$

The Kinetic Pathway 1 dominates micellar dynamics also in the concentration range $\phi > \phi_A$ because $k_BT\epsilon_{tot} < \Delta\mathscr{T}_e$ and the second part of eq 82 remains valid in this high concentration regime as well.

The terminal relaxation time, τ_h, is an exponentially increasing function of concentration in the region $\phi < \tilde{\phi}$ (both F_b and τ_{conf} are increasing with ϕ and $F_b \gg k_BT$). The behavior of terminal (hopping) time at higher concentrations (for the Kinetic Pathway 1) depends on the number of monomers between entanglements in the melt, N_{e0}, because the collective tube leakage time, τ_{conf}, increases with concentration, while phantom part of the deformation energy, $\Delta\mathscr{T}$, decreases with concentration. The concentration dependencies of these two competing contributions to the effective exponent, E, balance each other

$$m\left(\frac{\tilde{\phi}}{\phi_{min}}\right)^{1/[3(3\nu-1)]} \approx \left(\frac{\phi_{kink}}{\phi_e}\right)^{(1/3\nu-1)}\left(\frac{\phi_{min}}{\phi_{kink}}\right)^{2/[3(3\nu-1)]} \quad (83)$$

at concentration

$$\phi_{min} \approx \left(\frac{N_{e0}{}^{3/4}m^{3/2}}{l}\right)^{3\nu-1} \approx m^{3\nu-1}\phi_{kink} \approx \tilde{\phi}\left(\frac{N_{e0}}{m^{2/3}}\right)^{3/[4(3\nu-1)]} \quad (84)$$

The concentration dependence of the deformation energy, $\Delta\mathscr{T}$, dominates the effective exponent E at $\phi < \phi_{min}$, while the concentration dependence of the logarithm of the collective tube leakage time $\ln(\tau_{conf}/\tau_0)$ dominates at $\phi > \phi_{min}$. For $N_{e0} \lesssim m^{2/3}$ the concentration corresponding to the minimum is below the relevant range $\phi_{min} < \tilde{\phi}$ and the concentration dependence of the collective tube leakage time controls the hopping time, τ_h, in the concentration regime of overlapping micelles $\phi > \tilde{\phi}$. In this case, the terminal relaxation time is an exponentially increasing function in this concentration region as well (dotted line in Figure 9). In the case $m^{2/3} \lesssim N_{e0} \lesssim l^{4/3}/m^2$, the hopping time, τ_h, exponentially increases with concentration in the region $\phi^* < \phi < \tilde{\phi}$, then it exponentially decreases for $\tilde{\phi} < \phi < \phi_{min}$ because it is determined by the deformation energy. Finally, it increases again at higher concentrations, $\phi > \phi_{min}$, controlled by the tube leakage time (dashed and solid line in Figure 9). For $N_{e0} \gtrsim l^{4/3}/m^2$, the concentration corresponding to the minimum is $\phi_{min} > 1$ and the hopping time τ_h is an exponentially decreasing function of concentration in the whole concentration regime of overlapping micelles $\phi > \tilde{\phi}$ since it is dominated by the phantom part of the deformation energy, $\Delta\mathscr{T}$ (solid line in Figure 9).

Case B with $\min(m^{3/2}, m^3/N_{e0}) \lesssim \epsilon_{tot} \lesssim \max(m^{3/2}, m^3/N_{e0})$ can be split into two subcases: Case B′ for $N_e < m^{3/2}$ and Case B″ for $N_e > m^{3/2}$.

Case B′, $m^{3/2} \lesssim \epsilon_{tot} \lesssim m^3/N_{e0}$. This case is similar to Case A. The only difference is that concentration, ϕ_A, at which the entanglement part of the deformation energy, $\Delta\mathscr{T}_e$, is on the order of $k_BT\epsilon_{tot}$ is lower than concentration $\tilde{\phi}$. Concentration ϕ_A becomes the crossover between Kinetic Pathway 2 controlling micelle motion at lower concentrations and Kinetic Pathway 1

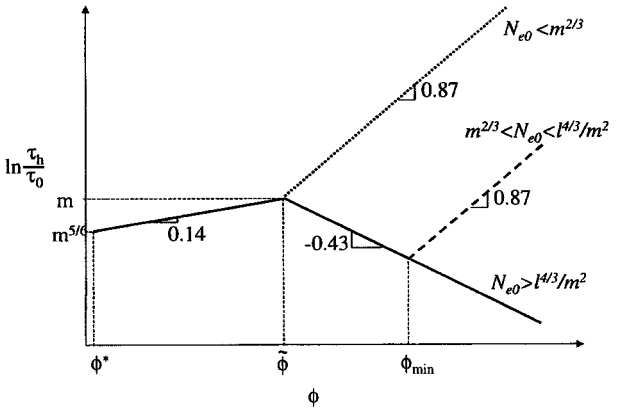

Figure 9. Concentration dependence of the logarithm of the terminal relaxation time (micelle hopping time), $E = \ln(\tau_h/\tau_0)$. Case A (or case B′ with ϕ_A replacing $\tilde{\phi}$). Logarithmic scales.

controlling it at higher concentrations.

$$E \approx \begin{cases} \dfrac{F_b}{k_BT} + \ln\dfrac{\tau_{conf}}{\tau_0} & \text{for } \phi < \phi_A \\ \dfrac{\Delta\mathscr{F}}{k_BT} + \ln\dfrac{\tau_{conf}}{\tau_0} & \text{for } \phi > \phi_A \end{cases} \tag{85}$$

Case B″, $m^3/N_{e0} \lesssim \epsilon_{tot} \lesssim m^{3/2}$. In this case, the hopping process controls the Kinetic Pathway 2 (eq 75) at low concentrations because $\Delta\mathscr{F}/(k_BT)$ is larger than ϵ_{tot} in the concentration range, $\phi^* < \phi < \phi_B$. The crossover concentration, ϕ_B, corresponds to debridging having comparable free energy barrier to hopping $\Delta\mathscr{F}(\phi_B) \approx k_BTm(\tilde{\phi}/\phi_B)^{1/[3(3\nu-1)]} \approx k_BT\epsilon_{tot}$.

$$\phi_B \approx \tilde{\phi}\left(\frac{m}{\epsilon_{tot}}\right)^{3(3\nu-1)} \tag{86}$$

This concentration is limited to the range $\phi^* < \phi_B < \tilde{\phi}(N_{e0}/m^2)^{3(3\nu-1)}$ in the case B″ (note that $\phi_B < \tilde{\phi}$ as $N_{e0} < m^2$). The low concentration regime ($\phi^* < \phi < \phi_B$) is dominated by the phantom part of deformation free energy, $\Delta\mathscr{F}(\phi) \approx k_BTm(\tilde{\phi}/\phi)^{1/[3(3\nu-1)]}$, and leads to an exponential decrease of the hopping time, τ_h, with concentration (essentially as $\tau_h \propto \exp(\text{const}\,\phi^{-0.43})$). The effective exponent is

$$E \approx \begin{cases} \dfrac{\Delta\mathscr{F}}{k_BT} + \ln\dfrac{\tau_m}{\tau_0} & \text{for } \phi^* < \phi < \phi_B \\ \dfrac{F_b}{k_BT} + \ln\dfrac{\tau_{conf}}{\tau_0} & \text{for } \phi_B < \phi < \tilde{\phi} \\ \dfrac{\Delta\mathscr{F}}{k_BT} + \ln\dfrac{\tau_{conf}}{\tau_0} & \text{for } \phi > \tilde{\phi} \end{cases} \tag{87}$$

The hopping time, τ_h, is exponentially increasing in the region, $\phi_B < \phi < \tilde{\phi}$, controlled by the debridging process. The behavior of E and τ_h in the region of overlapping micelles, $\phi > \tilde{\phi}$, is the same as in the Case A for $\epsilon_{tot} \gtrsim m^{3/2}$ and is nonmonotonic in the case $N_{e0} \lesssim l^{4/3}/m^2$: the hopping time, τ_h, exponentially decreases for $\tilde{\phi} < \phi < \phi_{min}$ (solid line in Figure 10) and increases at concentrations $\phi > \phi_{min}$ (dashed line in Figure 10). For $N_{e0} \gtrsim l^{4/3}/m^2$ the hopping time, τ_h, is an exponentially decreasing function in the entire concentration interval of overlapping micelles, $\phi > \tilde{\phi}$. The concentration dependence of the hopping time, $\tau_h(\phi)$, is shown schematically by a solid line in Figure 10. Note that the regime with $N_{e0} \lesssim m^{2/3}$ is not applicable because Case B″ exists only for $N_{e0} > m^{3/2}$.

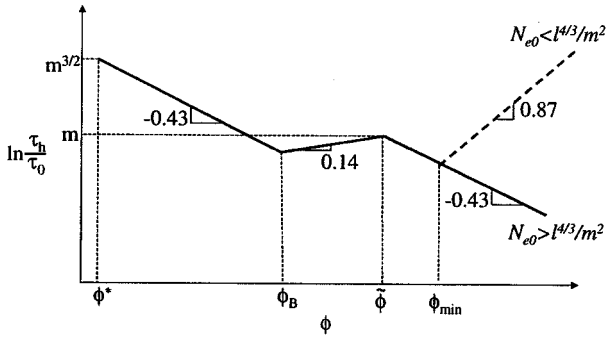

Figure 10. Concentration dependence of the logarithm of the terminal relaxation time (micelle hopping time), $E = \ln(\tau_h/\tau_0)$. Case B″ (or case C with ϕ_A replacing $\tilde{\phi}$). Logarithmic scales.

Case C, $m^{3/2}/N_{e0}^{1/4} \lesssim \epsilon_{tot} \lesssim \min(m^{3/2}, m^3/N_{e0})$. This case is similar to Case B″. The only difference is that concentration, ϕ_A, at which the entanglement part of the deformation energy, $\Delta\mathscr{F}_e$, is on the order of $k_BT\epsilon_{tot}$ is lower than concentration $\tilde{\phi}$. Concentration ϕ_A becomes the crossover between Kinetic Pathway 2 controlling micelle motion at intermediate concentrations and Kinetic Pathway 1 controlling it at higher concentrations.

$$E \approx \begin{cases} \dfrac{\Delta\mathscr{F}}{k_BT} + \ln\dfrac{\tau_m}{\tau_0} & \text{for } \phi^* < \phi < \phi_B \\ \dfrac{F_b}{k_BT} + \ln\dfrac{\tau_{conf}}{\tau_0} & \text{for } \phi_B < \phi < \phi_A \\ \dfrac{\Delta\mathscr{F}}{k_BT} + \ln\dfrac{\tau_{conf}}{\tau_0} & \text{for } \phi > \phi_A \end{cases} \tag{88}$$

Case D, $m(N_{e0}/m^2)^{1/8} < \epsilon_{tot} < m^{3/2}/N_{e0}^{1/4}$. For smaller activation energy ϵ_{tot} of sticker dissociation the deformation energy dominates the Kinetic Pathway 2 with $E_2 \approx F_a/k_BT + \ln(\tau_m/\tau_0)$. The effective exponent, E, is determined by the minimum of the corresponding terms of Kinetic Pathways 1 and 2.

$$E \approx \frac{\Delta\mathscr{F}}{k_BT} + \min\left\{\ln\frac{\tau_{conf}}{\tau_0}, \frac{\Delta\mathscr{F}_e + F_b}{k_BT} + \ln\frac{\tau_m}{\tau_0}\right\} \tag{89}$$

At low concentrations, the Kinetic Pathway 2 dominates the dynamics of micelles (see eq 77) because $\tau_m < \tau_{conf}$. At higher concentrations, the competition between the Kinetic Pathways 1 and 2 depends on the relative values of $\Delta\mathscr{F}_e/k_BT \approx m(\phi/\phi_e)^{1/(3\nu-1)}$ and ϵ_{tot}. These two terms are of the same order of magnitude at concentration ϕ_A. The effective exponent, E (eq 89), and the terminal relaxation time, τ_h, are controlled by the Kinetic Pathway 1 in the concentration range $\phi_A < \phi < 1$.

$$E \simeq \begin{cases} \dfrac{\Delta\mathscr{F} + \Delta\mathscr{F}_e}{k_BT} + \ln\dfrac{\tau_m}{\tau_0} & \text{for } \phi^* < \phi < \phi_A \\ \dfrac{\Delta\mathscr{F}}{k_BT} + \ln\dfrac{\tau_{conf}}{\tau_0} & \text{for } \phi_A < \phi < 1 \end{cases} \tag{90}$$

Terminal relaxation time, τ_h, decreases at lower concentrations ($\phi^* < \phi < \phi_A$) due to decreasing phantom part $\Delta\mathscr{F}$ of the deformation free energy in the Kinetic Pathway 2. The concentration behavior of terminal

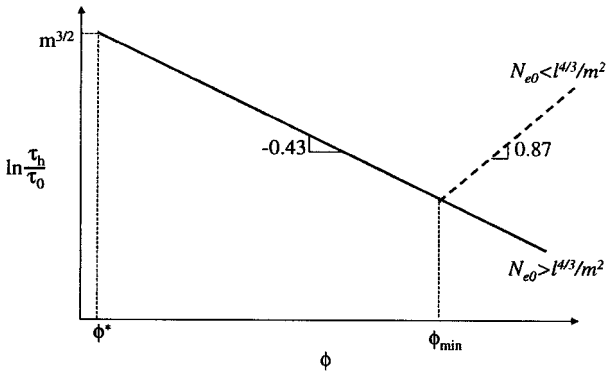

Figure 11. Concentration dependence of the logarithm of the terminal relaxation time (micelle hopping time), $E = \ln(\tau_h/\tau_0)$. Cases D, E, and F. Logarithmic scales.

relaxation time, τ_h, at higher concentrations $\phi > \phi_A$, controlled by the Kinetic Pathway 1, again depends on the degree of polymerization between entanglements N_{e0}. If $N_{e0} \gtrsim l^{4/3}/m^2$ the terminal relaxation time τ_h decreases with concentration for $\phi > \phi_A$ and therefore in the entire concentration interval (solid line in Figure 11). If $N_{e0} < l^{4/3}/m^2$, the hopping time, τ_h, decreases with ϕ for $\phi_A < \phi < \phi_{min}$ (solid line in Figure 11) and increases for $\phi > \phi_{min}$ (dashed line in Figure 11). The concentration, ϕ_{min}, corresponding to the hopping time minimum is defined in eq 84 and is higher than ϕ_A in this interval of ϵ_{tot}. Note that the concentration, ϕ_A (eq 81), is limited by $\phi_{be} < \phi_A < \phi_{kink}$ for sticker activation energy in the interval $m(N_{e0}/m^2)^{1/8} < \epsilon_{tot} < m^{3/2}/N_{e0}^{1/4}$, where the lower bound concentration

$$\phi_{be} \approx \phi_e \left(\frac{N_{e0}}{m^2}\right)^{(3\nu-1)/8} \tag{91}$$

corresponds to the entanglement part of the deformation energy, $\Delta\mathcal{F}_e$, on the order of the energy penalty for debridging F_b.

Case E. For even lower ϵ_{tot}, $m^{5/6} < \epsilon_{tot} < m(N_{e0}/m^2)^{1/8}$, the effective exponent, E, is again determined by the minimum of eq 89. In this case the competition between the Kinetic Pathways 1 and 2 depends on the relative value of debridging free energy penalty $F_b/k_BT \approx m(\phi/\tilde{\phi})^{1/[9(3\nu-1)]}$ and ϵ_{tot}. These two terms are of the same order of magnitude at concentration

$$\phi_E \approx \tilde{\phi}\left(\frac{\epsilon_{tot}}{m}\right)^{9(3\nu-1)} \tag{92}$$

The effective exponent, E (eq 89), and the terminal relaxation time, τ_h, are controlled by the Kinetic Pathway 2 in the concentration range $\phi^* < \phi < \phi_E$ and by the Kinetic Pathway 1 in the concentration range $\phi_E < \phi < 1$.

$$E \approx \begin{cases} \dfrac{\Delta\mathcal{F} + \Delta F_b}{k_BT} + \ln\dfrac{\tau_m}{\tau_0} & \text{for } \phi^* < \phi < \phi_E \\ \dfrac{\Delta\mathcal{F}}{k_BT} + \ln\dfrac{\tau_{conf}}{\tau_0} & \text{for } \phi_E < \phi < 1 \end{cases} \tag{93}$$

The concentration behavior of the hopping time, τ_h, is qualitatively similar to that of the regime, $m(N_{e0}/m^2)^{1/8} < \epsilon_{tot} < m^{3/2}/N_{e0}^{1/4}$ (see Figure 11).

Case F. For the smallest values of the activation energy of sticker dissociation, $m^{1/2} < \epsilon_{tot} < m^{5/6}$, the Kinetic Pathway 1 dominates the motion of micelles in the entire concentration range.

$$E \approx \frac{\Delta\mathcal{F}}{k_BT} + \ln\frac{\tau_{conf}}{\tau_0} \quad \text{for } \phi^* < \phi < 1 \tag{94}$$

The concentration behavior of the terminal relaxation time is similar to that of the above regimes, $m^{5/6} < \epsilon_{tot} < m^{3/2}/N_{e0}^{1/4}$ (see Figure 11). Note that the micellar hopping time, τ_h, as defined in eqs 60 and 77 is always (much) longer than chain conformation relaxation time, τ_{conf} (eq 59).[24]

4.2. The Stress Relaxation and the Viscosity. The stress relaxation after an infinitesimal shear is defined by the relaxation modulus, $G(t)$. A fraction of the stress associated with orientation of bridges and entanglements is relaxing during the time, τ_{conf}. The corresponding shear modulus (in the regime of entanglements) is $G_e \approx k_BT\phi/N_e(\phi)$. Another contribution to the stress (induced by the shear) is due to deformation of micellar cells. The corresponding elastic (shear) modulus, G_m, is defined in eq 31. Relaxation of the micellar stress must involve micellar hops and the corresponding relaxation time is on the order of τ_h. The relaxation modulus can be roughly represented as

$$G(t) \approx G_e e^{-t/\tau_{conf}} + G_m e^{-t/\tau_h} \tag{95}$$

The zero-shear-rate viscosity of the reversible micellar gel is

$$\eta = \int G(t)\,dt \approx G_e\tau_{conf} + G_m\tau_h \tag{96}$$

The micellar hopping time, τ_h, is exponentially longer than τ_{conf} (see the previous section), hence, relaxation of micelles dominates the zero-shear-rate viscosity.

$$\eta \approx G_m\tau_h \tag{97}$$

5. Summary of the Main Results

Below, we summarize the main results of the theory presented in the previous sections. We assume four conditions: eqs 11, 32, 34, and 46. We distinguish the following five concentration regimes:

(a) unentangled reversible gel in concentration range $\phi^* < \phi < \phi_e^*$, (b) weakly entangled gel with unentangled l-spacers at concentrations $\phi_e^* < \phi < \phi_e$, (c) strongly entangled gel of segregated micelles with transport by unentangled loops at $\phi_e < \phi < \phi_{kink}$, (d) strongly entangled gel of segregated micelles with collective tube leakage transport at $\phi_{kink} < \phi < \tilde{\phi}$, (e) strongly entangled gel of overlapping micelles with collective tube leakage transport at concentrations $\tilde{\phi} < \phi < 1$.

The crossover concentrations are: overlap of micelles ϕ^* (eq 9), entanglement of chains ϕ_e^* (eq 41), entanglement of l-spacers ϕ_e (eq 42), crossover between transport by unentangled loops and by collective tube leakage ϕ_{kink} (eq 53), and crossover between segregated and overlapping micelles $\tilde{\phi}$ (eq 22).

$$\phi^* \sim \left(\frac{m^{1/2}}{l}\right)^{3\nu-1};\ \phi_e^* \sim \left(\frac{N_{e0}}{lf}\right)^{3\nu-1};\ \phi_e \sim \left(\frac{N_{e0}}{l}\right)^{3\nu-1};$$
$$\phi_{kink} \approx \left(\frac{N_{e0}^{3/4}m^{1/2}}{l}\right)^{3\nu-1};\ \tilde{\phi} \sim \left(\frac{m^2}{l}\right)^{3\nu-1} \tag{98}$$

5.1. The Conformation Relaxation Time. The relaxation time of chain conformations in different regimes is (see eq 59 and Figure 6)

$$\tau_{conf} \approx \tau_b f^2 \approx \tau_0 e^{\epsilon+\epsilon_a} f^2 \quad \text{for } \phi^* < \phi < \phi_e{}^* \tag{99}$$

$$\tau_{conf} \approx \tau_b f^3 \frac{F_e}{k_B T} \approx \tau_0 e^{\epsilon+\epsilon_a} f^3 \left(\frac{\phi}{\phi_e}\right)^{1/(3\nu-1)} \quad \text{for } \phi_e{}^* < \phi < \phi_e \tag{100}$$

$$\tau_{conf} \approx \tau_b f^3 \exp\left(\frac{F_e}{k_B T}\right) \approx \tau_0 e^{\epsilon+\epsilon_a} f^3 \exp\left[\left(\frac{\phi}{\phi_e}\right)^{1/(3\nu-1)}\right] \quad \text{for } \phi_e < \phi < \phi_{kink} \tag{101}$$

$$\tau_{conf} \approx \tau_b f^3 \exp\left(\frac{F^*}{k_B T}\right)$$

$$\approx \tau_0 e^{\epsilon+\epsilon_a} f^3 \exp\left[\left(\frac{\phi_{kink}}{\phi_e}\right)^{1/(3\nu-1)} \left(\frac{\phi}{\phi_{kink}}\right)^{2/[3(3\nu-1)]}\right] \quad \text{for } \phi_{kink} < \phi \tag{102}$$

where bond lifetime, $\tau_b = \tau_0 e^{\epsilon+\epsilon_a}$ (eq 35), free energy of an entangled l-spacer, $F_e \approx k_B T(\phi/\phi_e)^{1/(3\nu-1)}$ (eq 44), and free energy of a collective kink $F^* \approx k_B T(\phi_{kink}/\phi_e)^{1/(3\nu-1)} (\phi/\phi_{kink})^{2/[3(3\nu-1)]}$ (eq 55). The relaxation is always slow due to the exponential factor e^{ϵ}, where $\epsilon k_B T$ is the sticker dissociation energy. The conformation relaxation time is thus nearly constant in the unentangled regime, it then increases as $\phi^{1.3}$ in the weakly entangled regime. At higher concentrations, τ_{conf} increases exponentially first as $\tau_{conf} \sim \exp(\text{const } \phi^{1.3})$ and finally as $\tau_{conf} \sim \exp(\text{const } \phi^{0.87})$.

This exponential growth of the conformational relaxation time in regimes with entangled l-spacers is much stronger than the power-law concentration dependence of the chain relaxation time with different exponents (depending on the regime) that was predicted for reversible gels with pairwise association of stickers.[7,8] The exponential dependence in the strongly entangled regimes (c, d, and e) can be interpreted as a power law with indefinitely increasing effective exponent.

5.2. Self-Diffusion Constant. During the time τ_{conf} an associating polymer chain typically moves by a distance of the order of its own size, R_N, as defined in eq 33. The chain self-diffusion constant is then

$$D_N \approx \frac{R_N{}^2}{\tau_{conf}}$$

D_N is weakly decreasing with concentration in regimes (a, b); however, the diffusion slows down exponentially in the strongly entangled regimes (c − e).

5.3. The Stress Relaxation Time and the Viscosity. Terminal relaxation of the reversible network formed by interconnected micelles proceeds by hopping of these micelles. This motion of micelles can follow two possible kinetic pathways. In the Kinetic Pathway 1, the system is relaxed at any moment of the hopping process. In the Kinetic Pathway 2, micelles prepare for the jump by transforming all old bridges into the loops. The fastest of the two pathways controls the dynamics of the reversible network.

Both the terminal stress relaxation time and the viscosity are proportional to $\tau_h = \tau_0 e^E$, where effective exponent $E \gg 1$ depends on polymer volume fraction ϕ. Hence,

$$\ln \frac{\eta}{\eta_s} \approx \ln \frac{\tau_h}{\tau_0} + \ln\left(\frac{G_m}{k_B T/b^3}\right) \approx E + \ln\left(\frac{G_m}{k_B T/b^3}\right)$$

$$\approx E + \ln\left[\frac{\phi}{l}\left(\frac{\tilde{\phi}}{\phi}\right)^{1/[3(3\nu-1)]}\right] \tag{103}$$

where η_s is the solvent viscosity. Modulus G_m increases as a power of concentration, $G \sim \phi^{0.57}$ (eq 31), and therefore makes a logarithmic contribution to $\ln(\eta/\eta_s)$. The effective exponent, E (eq 77), was estimated in the previous section. The result depends on the relative value of the activation energy ϵ_{tot} of sticker dissociation.

Case A. For very high activation energy of sticker dissociation $\epsilon_{tot} \gtrsim \max(m^{3/2}, m^3/N_{e0})$ our predictions are

$$\ln\frac{\eta}{\eta_s} \approx \ln\frac{\tau_h}{\tau_0} \approx E \approx \begin{cases} \dfrac{F_b}{k_BT} + \ln\dfrac{\tau_{conf}}{\tau_0} & \text{for } \phi < \tilde{\phi} \\ \dfrac{\Delta\mathscr{F}}{k_BT} + \ln\dfrac{\tau_{conf}}{\tau_0} & \text{for } \phi > \tilde{\phi} \end{cases}$$

$$\approx \begin{cases} m\left(\dfrac{\phi}{\tilde{\phi}}\right)^{1/[9(3\nu-1)]} + \epsilon_{tot} & \text{for } \phi < \phi_e \\ m\left(\dfrac{\phi}{\tilde{\phi}}\right)^{1/[9(3\nu-1)]} + \epsilon_{tot} + \left(\dfrac{\phi}{\phi_e}\right)^{1/(3\nu-1)} & \text{for } \phi_e < \phi < \phi_{kink} \\ m\left(\dfrac{\phi}{\tilde{\phi}}\right)^{1/[9(3\nu-1)]} + \epsilon_{tot} + \left(\dfrac{\phi_{kink}}{\phi_e}\right)^{1/(3\nu-1)}\left(\dfrac{\phi}{\phi_{kink}}\right)^{2/[3(3\nu-1)]} & \text{for } \phi_{kink} < \phi < \tilde{\phi} \\ m\left(\dfrac{\tilde{\phi}}{\phi}\right)^{1/[3(3\nu-1)]} + \epsilon_{tot} + \left(\dfrac{\phi_{kink}}{\phi_e}\right)^{1/(3\nu-1)}\left(\dfrac{\phi}{\phi_{kink}}\right)^{2/[3(3\nu-1)]} & \text{for } \phi > \tilde{\phi} \end{cases}$$

At lower concentrations, $\phi < \tilde{\phi}$, micelles move via Kinetic Pathway 2 dominated by the debridging mechanism. Both viscosity and terminal relaxation time increase as an exponential of a power of concentration (solid line in Figure 9). At higher concentrations $\phi > \tilde{\phi}$ micelles move via Kinetic Pathway 1. The concentration dependence of micelle dynamics depends on the relative value of the number of monomers between entanglements N_{e0}.

(*i*) For large relative values of $N_{e0} > l^{4/3}/m^2$ both terminal relaxation time and solution viscosity are nonmonotonic and decrease in the concentration range $\phi > \tilde{\phi}$, controlled by the Kinetic Pathway 1 (see solid line in Figure 9).

$$\eta \sim \tau_h \sim \exp(\text{const}\ \phi^{-0.43}) \tag{104}$$

This anomalous decrease of viscosity and terminal relaxation time is due to the fact that the concentration dependence of relaxation is controlled by the phantom part, $\Delta\mathscr{F}$, of the deformation energy of micelles that decreases with concentration (eq 61).

(*ii*) For intermediate relative values of the number of monomers between entanglements, $m^{2/3} < N_{e0} < l^{4/3}/m^2$, both viscosity and terminal relaxation time decrease in the concentration range, $\tilde{\phi} < \phi < \phi_{min}$ (eq 104), and increase at higher concentrations $\phi > \phi_{min}$

$$\eta \sim \tau_h \sim \exp(\text{const}\ \phi^{0.87}) \tag{105}$$

with the concentration corresponding to the minimum given by eq 84 (solid and dashed line in Figure 9).

(*iii*) For small $N_{e0} < m^{2/3}$, the dynamics is controlled by the collective tube leakage with viscosity and terminal relaxation time increasing at all concentrations (see dotted line in Figure 9).

Case B′. $m^{3/2} \lesssim \epsilon_{tot} \lesssim m^3/N_{e0}$. This regime is similar to Case A, with concentration ϕ_A (eq 81) replacing concentration $\tilde{\phi}$.

$$\ln\frac{\eta}{\eta_s} \approx \ln\frac{\tau_h}{\tau_0} \approx E \approx \begin{cases} \dfrac{F_b}{k_BT} + \ln\dfrac{\tau_{conf}}{\tau_0} & \text{for } \phi < \phi_A \\ \dfrac{\Delta\mathscr{F}}{k_BT} + \ln\dfrac{\tau_{conf}}{\tau_0} & \text{for } \phi > \phi_A \end{cases}$$

$$\approx \begin{cases} m\left(\dfrac{\phi}{\tilde{\phi}}\right)^{1/[9(3\nu-1)]} + \epsilon_{tot} & \text{for } \phi < \phi_e \\ m\left(\dfrac{\phi}{\tilde{\phi}}\right)^{1/[9(3\nu-1)]} + \epsilon_{tot} + \left(\dfrac{\phi}{\phi_e}\right)^{1/(3\nu-1)} & \text{for } \phi_e < \phi < \phi_{kink} \\ m\left(\dfrac{\phi}{\tilde{\phi}}\right)^{1/[9(3\nu-1)]} + \epsilon_{tot} + \left(\dfrac{\phi_{kink}}{\phi_e}\right)^{1/(3\nu-1)}\left(\dfrac{\phi}{\phi_{kink}}\right)^{2/[3(3\nu-1)]} & \text{for } \phi_{kink} < \phi < \phi_A \\ m\left(\dfrac{\tilde{\phi}}{\phi}\right)^{1/[3(3\nu-1)]} + \epsilon_{tot} + \left(\dfrac{\phi_{kink}}{\phi_e}\right)^{1/(3\nu-1)}\left(\dfrac{\phi}{\phi_{kink}}\right)^{2/[3(3\nu-1)]} & \text{for } \phi > \phi_A \end{cases}$$

Case B″**.** In regime $m^3/N_{e0} \lesssim \epsilon_{tot} \lesssim m^{3/2}$, we predict

$$\ln\frac{\eta}{\eta_s} \approx \ln\frac{\tau_h}{\tau_0} \approx E \approx \begin{cases} \dfrac{\Delta\mathscr{F}}{k_BT} + \ln\dfrac{\tau_m}{\tau_0} & \text{for } \phi^* < \phi < \phi_B \\ \dfrac{F_b}{k_BT} + \ln\dfrac{\tau_{conf}}{\tau_0} & \text{for } \phi_B < \phi < \tilde{\phi} \\ \dfrac{\Delta\mathscr{F}}{k_BT} + \ln\dfrac{\tau_{conf}}{\tau_0} & \text{for } \phi > \tilde{\phi} \end{cases}$$

$$\approx \begin{cases} m\left(\dfrac{\tilde{\phi}}{\phi}\right)^{1/[3(3\nu-1)]} & \text{for } \phi^* < \phi < \phi_B \\ m\left(\dfrac{\phi}{\tilde{\phi}}\right)^{1/[9(3\nu-1)]} + \epsilon_{tot} + \left(\dfrac{\phi}{\phi_e}\right)^{1/(3\nu-1)} & \text{for } \phi_B < \phi < \phi_{kink} \\ m\left(\dfrac{\phi}{\tilde{\phi}}\right)^{1/[9(3\nu-1)]} + \epsilon_{tot} + \left(\dfrac{\phi_{kink}}{\phi_e}\right)^{1/(3\nu-1)}\left(\dfrac{\phi}{\phi_{kink}}\right)^{2/[3(3\nu-1)]} & \text{for } \phi_{kink} < \phi < \tilde{\phi} \\ m\left(\dfrac{\tilde{\phi}}{\phi}\right)^{1/[3(3\nu-1)]} + \epsilon_{tot} + \left(\dfrac{\phi_{kink}}{\phi_e}\right)^{1/(3\nu-1)}\left(\dfrac{\phi}{\phi_{kink}}\right)^{2/[3(3\nu-1)]} & \text{for } \phi > \tilde{\phi} \end{cases}$$

In this case, viscosity and relaxation time decrease at low concentrations for $\phi^* < \phi < \phi_B$ (eq 104), where concentration ϕ_B is defined by eq 86. This decrease is due to the hopping part of the Kinetic Pathway 2. At higher concentrations (for $\phi > \phi_B$), the dynamics is similar to the Case A above with $\epsilon_{tot} > m^{3/2}$. For $N_{e0} < l^{4/3}/m^2$, there are two concentrations regimes ($\phi^* < \phi < \phi_B$ and $\tilde{\phi} < \phi < \phi_{min}$) with decreasing viscosity and relaxation time (solid lines in Figure 10) and two concentration regimes ($\phi_B < \phi < \tilde{\phi}$ and $\phi > \phi_{min}$) with increasing viscosity and relaxation time (solid and dashed lines Figure 10). For $N_{e0} \gtrsim l^{4/3}/m^2$, both viscosity and relaxation time exponentially decrease at low and high concentrations ($\phi^* < \phi < \phi_B$ and $\phi > \tilde{\phi}$) and exponentially increase in the intermediate concentration range ($\phi_B < \phi < \tilde{\phi}$) as shown by solid lines in Figure 10.

Case C. $m^{3/2}/N_{e0}^{1/4} \lesssim \epsilon_{tot} \lesssim \min(m^{3/2}, m^3/N_{e0})$. This regime is similar to Case B″ with concentration ϕ_A (eq 81) replacing concentration $\tilde{\phi}$ as the highest boundary between concentration regimes.

$$\ln\frac{\eta}{\eta_s} \approx \ln\frac{\tau_h}{\tau_0} \approx E \approx \begin{cases} \dfrac{\Delta\mathscr{F}}{k_BT} + \ln\dfrac{\tau_m}{\tau_0} & \text{for } \phi^* < \phi < \phi_B \\ \dfrac{F_b}{k_BT} + \ln\dfrac{\tau_{conf}}{\tau_0} & \text{for } \phi_B < \phi < \phi_A \\ \dfrac{\Delta\mathscr{F}}{k_BT} + \ln\dfrac{\tau_{conf}}{\tau_0} & \text{for } \phi > \phi_A \end{cases}$$

$$\approx \begin{cases} m\left(\dfrac{\tilde{\phi}}{\phi}\right)^{1/[3(3\nu-1)]} & \text{for } \phi^* < \phi < \phi_B \\ m\left(\dfrac{\phi}{\tilde{\phi}}\right)^{1/[9(3\nu-1)]} + \epsilon_{tot} + \left(\dfrac{\phi}{\phi_e}\right)^{1/(3\nu-1)} & \text{for } \phi_B < \phi < \phi_{kink} \\ m\left(\dfrac{\phi}{\tilde{\phi}}\right)^{1/[9(3\nu-1)]} + \epsilon_{tot} + \left(\dfrac{\phi_{kink}}{\phi_e}\right)^{1/(3\nu-1)}\left(\dfrac{\phi}{\phi_{kink}}\right)^{2/[3(3\nu-1)]} & \text{for } \phi_{kink} < \phi < \phi_A \\ m\left(\dfrac{\tilde{\phi}}{\phi}\right)^{1/[3(3\nu-1)]} + \epsilon_{tot} + \left(\dfrac{\phi_{kink}}{\phi_e}\right)^{1/(3\nu-1)}\left(\dfrac{\phi}{\phi_{kink}}\right)^{2/[3(3\nu-1)]} & \text{for } \phi > \phi_A \end{cases}$$

Case D. For intermediate activation energy of sticker dissociation, $m(N_{e0}/m^2)^{1/8} \lesssim \epsilon_{tot} \lesssim m^{3/2}/N_{e0}^{1/4}$, our results are

$$\ln\frac{\eta}{\eta_s} \approx \ln\frac{\tau_h}{\tau_0} \approx E \approx \begin{cases} \dfrac{\Delta\mathscr{F} + \Delta\mathscr{F}_e}{k_BT} + \ln\dfrac{\tau_m}{\tau_0} & \text{for } \phi^* < \phi < \phi_A \\ \dfrac{\Delta\mathscr{F}}{k_BT} + \ln\dfrac{\tau_{conf}}{\tau_0} & \text{for } \phi_A < \phi < 1 \end{cases}$$

$$\approx \begin{cases} m\left(\dfrac{\tilde{\phi}}{\phi}\right)^{1/[3(3\nu-1)]} + m\left(\dfrac{\phi}{\phi_e}\right)^{1/(3\nu-1)} & \text{for } \phi^* < \phi < \phi_A \\ m\left(\dfrac{\tilde{\phi}}{\phi}\right)^{1/[3(3\nu-1)]} + \epsilon_{tot} + \left(\dfrac{\phi}{\phi_e}\right)^{1/(3\nu-1)} & \text{for } \phi_A < \phi < \phi_{kink} \\ m\left(\dfrac{\tilde{\phi}}{\phi}\right)^{1/[3(3\nu-1)]} + \epsilon_{tot} + \left(\dfrac{\phi_{kink}}{\phi_e}\right)^{1/(3\nu-1)}\left(\dfrac{\phi}{\phi_{kink}}\right)^{2/[3(3\nu-1)]} & \text{for } \phi_{kink} < \phi < 1 \end{cases}$$

where the concentration, ϕ_A, is given by eq 81. At lower concentrations ($\phi^* < \phi < \phi_A$), the dynamics of micelles is controlled by the Kinetic Pathway 2 with both viscosity and terminal relaxation time decreasing with concentration (eq 104). This decrease is due to dominance of the phantom part, $\Delta\mathscr{T}$, of the deformation energy. At higher concentrations ($\phi > \phi_A$), the dynamics is determined by the Kinetic Pathway 1.

(*i*) For large relative values of the number of monomers between entanglements, $N_{e0} > l^{4/3}/m^2$, both terminal relaxation time and solution viscosity decrease in the whole concentration range $\phi > \phi_A$. This is controlled by the Kinetic Pathway 1 (see eq 104) and therefore decreases in the entire concentration range, $\phi > \phi^*$ (solid line in Figure 11).

(*ii*) For low relative values of $N_{e0} < l^{4/3}/m^2$, the viscosity and terminal relaxation time decrease in the concentration range $\phi_A < \phi < \phi_{min}$ (eq 104) and increase at higher concentrations, $\phi > \phi_{min}$ (eq 105) (dashed line in Figure 11). The concentration ϕ_{min}, corresponding to the minimum (eq 84), is always larger than ϕ_A.

Case E. For smaller activation energy of sticker dissociation $m^{5/6} \lesssim \epsilon_{tot} \lesssim m(N_{e0}/m^2)^{1/8}$ we find

$$\ln\frac{\eta}{\eta_s} \approx \ln\frac{\tau_h}{\tau_0} \approx E \approx \begin{cases} \dfrac{\Delta\mathscr{T}+\Delta F_b}{k_BT} + \ln\dfrac{\tau_m}{\tau_0} & \text{for } \phi^* < \phi < \phi_E \\ \dfrac{\Delta\mathscr{T}}{k_BT} + \ln\dfrac{\tau_{conf}}{\tau_0} & \text{for } \phi_E < \phi < 1 \end{cases}$$

$$\approx \begin{cases} m\left(\dfrac{\tilde\phi}{\phi}\right)^{1/[3(3\nu-1)]} + m\left(\dfrac{\phi}{\tilde\phi}\right)^{1/[9(3\nu-1)]} & \text{for } \phi^* < \phi < \phi_E \\ m\left(\dfrac{\tilde\phi}{\phi}\right)^{1/[3(3\nu-1)]} + \epsilon_{tot} + \left(\dfrac{\phi}{\phi_e}\right)^{1/(3\nu-1)} & \text{for } \phi_E < \phi < \phi_{kink} \\ m\left(\dfrac{\tilde\phi}{\phi}\right)^{1/[3(3\nu-1)]} + \epsilon_{tot} + \left(\dfrac{\phi_{kink}}{\phi_e}\right)^{1/(3\nu-1)}\left(\dfrac{\phi}{\phi_{kink}}\right)^{2/[3(3\nu-1)]} & \text{for } \phi_{kink} < \phi < 1 \end{cases}$$

where the concentration ϕ_E is given in eq 92. The concentration dependence of viscosity and terminal relaxation time is qualitatively similar to the case D above (see Figure 11).

Case F. For $m^{1/2} < \epsilon_{tot} < m^{5/6}$, the micellar motion proceeds via the Kinetic Pathway 1. Viscosity and terminal relaxation time in this case are

$$\ln\frac{\eta}{\eta_s} \approx \ln\frac{\tau_h}{\tau_0} \approx E \approx \frac{\Delta\mathscr{T}}{k_BT} + \ln\frac{\tau_{conf}}{\tau_0} \qquad \text{for } \phi^* < \phi < 1$$

$$\approx \begin{cases} m\left(\dfrac{\tilde\phi}{\phi}\right)^{1/[3(3\nu-1)]} + \epsilon_{tot} + \left(\dfrac{\phi}{\phi_e}\right)^{1/(3\nu-1)} & \text{for } \phi < \phi_{kink} \\ m\left(\dfrac{\tilde\phi}{\phi}\right)^{1/[3(3\nu-1)]} + \epsilon_{tot} + \left(\dfrac{\phi_{kink}}{\phi_e}\right)^{1/(3\nu-1)}\left(\dfrac{\phi}{\phi_{kink}}\right)^{2/[3(3\nu-1)]} & \text{for } \phi > \phi_{kink} \end{cases} \tag{106}$$

The concentration behavior of the terminal relaxation time is similar to that of the above regimes $m^{5/6} < \epsilon_{tot} < m^{3/2}/N_{e0}^{1/4}$:

(*i*) For $N_{e0} > l^{4/3}/m^2$ both terminal relaxation time and solution viscosity decrease at all concentrations ($\phi^* < \phi < 1$) (see eq 104) as sketched by a solid line in Figure 11.

(*ii*) For $N_{e0} < l^{4/3}/m^2$ the viscosity and terminal relaxation time decrease in the concentration range $\phi^* < \phi < \phi_{min}$ (eq 104) and increase at higher concentrations $\phi > \phi_{min}$ (eq 105) (dashed line in Figure 11). This is a typical regime for $\epsilon_{tot} \cong 25$, $m \cong 50 \div 100$, $N_{e0} \cong 20 \div 100$. Other regimes are possible for smaller m.

6. Discussion

In this paper we investigated both single-chain and collective dynamics in reversible gels formed in associating polymer solutions. Linear polymers with stickers forming large aggregates are considered. Hence, the reversible gelation is a (strong) first-order transition resulting in a phase of closely packed micelles connected by bridging chain fragments (Figure 2). The chain and micellar dynamics in this phase are very slow even at the lowest concentration ϕ^*. The dynamics are always hindered by the high energy penalty for a sticker dissociation.

The present theory may be considered as an extension of the previous theoretical studies[7,8] on dynamics of polymers with pairwise association of stickers. One of the most important results is that (in the case of large aggregates) the stress relaxation time is much longer than the single-chain relaxation time (conformational relaxation time).[24] The reason is that the stress relaxation time is determined by the time of micellar positional rearrangements which are very slow as high free energy barriers are involved. Hence, chain diffusion is much (exponentially) faster than the stress relaxation: a polymer chain can typically diffuse by many of its diameters during the stress relaxation time.[10]

We predict that the chain conformational relaxation time, τ_{conf}, exhibits a relatively weak (power-law) increase with concentration ϕ in weakly entangled regime at lower concentrations ($\phi < \phi_e$). A much stronger exponential increase is predicted at higher concentra-

tions ($\phi > \phi_e$) when the soluble spacers are strongly entangled. This behavior is in contrast with the power-law increase of τ_{conf} predicted in all concentration regimes in the case of pairwise association.[7,8]

The present theory can be also considered as a generalization of the previous theory[9] on dynamics of micellar (reversible) gels formed in solutions of telechelic polymers. In this regard, we considered associating polymers with many (f) stickers rather than just two stickers per chain, extended the theory to the high concentration regime ($\phi > \tilde{\phi}$), where the bridges are typically connecting distant micelles (rather than the nearest neighbors) and took into account the effect of entanglements. There are two more parameters (f and N_e) in addition to the aggregation number m, the soluble spacer length l, the sticker binding energy ϵ, etc. It is therefore not surprising that with that many parameters we identified numerous regimes of different concentration behaviors of the stress relaxation time and the viscosity η.

The most complicated behavior (see Figure 10) is revealed for intermediate sticking energies and for intermediate entanglement densities: after an initial increase of the viscosity, η, due to the micellar gel formation at $\phi \sim \phi^*$ (this regime is not considered in the paper and is not illustrated in Figure 10), η starts to *decrease* exponentially with concentration ϕ, then (at intermediate concentrations) η shows a strong (exponential) increase, then it sharply decreases again (at $\phi > \tilde{\phi}$) and shows the final increase at the highest concentrations. In all the cases, the anomalous decrease of viscosity with concentration is due to the fact that the micellar deformation energy (that happens to determine the activation barrier for micellar hops) is a decreasing function of concentration. The soluble fragments forming a micellar corona are less stretched for higher concentrations, hence, lower deformation energy defined by the elastic energy of stretching. The final increase of viscosity at the highest concentrations is due to the increasing entanglement contribution to the micellar activation energy.

The predicted strong effects (exponential concentration dependencies of the viscosity and relaxation times) justify the plausibility of the crude approach to dynamics of micellar rearrangements (scaling estimates for the activation barriers) adopted in this paper.

It is worth noting that rather strong concentration dependencies of the viscosity were also predicted for systems with pairwise association ($m = 2$) of stickers.[7,8] However, these dependencies are scaling power laws; they are never exponential. Besides, the physical origin of the effect is entirely different in the pairwise association case ($m = 2$) from the case of large aggregates considered in the present paper ($m \gg 1$). For $m = 2$, an increase of viscosity is (in particular) due to a considerable depletion of open stickers resulting in multiple repeated reassociations of the same pair of stickers. This effect is much less important for large aggregation numbers $m \gg 1$. The predicted, exponentially slow (concentration dependent) dynamics of associating polymers with $m \gg 1$ is due to strongly interacting bulky micelles that may also trap entanglements.

We hope that our unexpected predictions of nonmonotonic concentration dependence of viscosity and terminal relaxation time will stimulate systematic experimental study of these interesting polymeric systems.

Acknowledgment. M.R. acknowledges support of NSF Grants DMR-0102267 and ECS-0103307, as well of the donors of the Petroleum Research Fund, administered by the American Chemical Society for partial support of this research. A.N.S. also acknowledges partial support from NATO SfP Grant 974173.

References and Notes

(1) Regulado, E. J.; Selb J.; Candau, F. *Macromolecules* **1999**, *32*, 8580.
(2) Williams, C. E. In *Multiphase Macromolecular Systems*; Culbertson, B. M., Ed.; Plenum Press: New York, 1989; Vol. 6.
(3) Moore, R. B.; Bittencourt, D.; Gauthier, M.; Williams, C. E.; Eisenberg, A. *Macromolecules* **1991**, *24*, 1376.
(4) Broze, G.; Jerome, R.; Teyssie, P. *Macromolecules* **1983**, *16*, 996.
(5) Balsara, N. P.; Tirrel, M.; Lodge, T. P. *Macromolecules* **1991**, *24*, 1975.
(6) Semenov, A. N.; Rubinstein, M. *Macromolecules* **1998**, *31*, 1373.
(7) Rubinstein, M.; Semenov, A. N. *Macromolecules* **1998**, *31*, 1386.
(8) Rubinstein, M.; Semenov, A. N. Macromolecules **2001**, *34*, 1058.
(9) Semenov, A. N.; Joanny, J.-F.; Khokhlov, A. R. *Macromolecules* **1995**, *28*, 1066.
(10) Leibler, L.; Rubinstein, M.; Colby, R. H. *J. Phys. II* **1993**, *3*, 1581. Stress relaxation in associating telechelic ionomers is predicted to be much slower than diffusion time of individual chains. The physical reason for this anomaly is qualitatively different from the exponentially slow micellar hopping analyzed in the present paper.
(11) Halperin, A.; Tirrell, M.; Lodge, T. P. *Adv. Polym. Sci.* **1992**, *100*, 31.
(12) Birshtein, T. M.; Zhulina, E. B. *Polymer* **1989**, *30*, 170.
(13) Eisenberg, A. *Macromolecules* **1970**, *3*, 147. Nyrkova, I. A.; Khokhlov, A. R.; Doi, M. *Macromolecules* **1993**, *26*, 3601. Semenov, A. N.; Nyrkova, I. A.; Khokhlov, A. R. *Macromolecules* **1995**, *28*, 7491. Semenov, A. N.; Nyrkova I. A.; Khokhlov A. R. Statistics and Dynamics of Ionomers In *Ionomers: Characterization, Theory and Applications*; Schlick, S., Ed.; CRC Press: New York, 1996.
(14) Daoud, M.; Cotton, J. P. *J. Phys. (Paris)* **1982**, *43*, 531.
(15) Birshtein, T.; Zhulina, E. *Polymer* **1984**, *25*, 1453.
(16) Witten, T. A.; Pincus, P. A. *Macromolecules* **1986**, *19*, 2509.
(17) Birshtein, T.; Zhulina, E.; Borisov, O. *Polymer* **1986**, *27*, 1078.
(18) De Gennes, P. G. *Scaling Concepts in Polymer Physics,* 2nd ed.; Cornell University Press: Ithaca, NY, 1985.
(19) Panyukov, S. V. *Sov. Phys.—JETP (Engl. Transl.)* **1990**, *71*, 372.
(20) Semenov, A. N. *Sov. Phys.—JETP* **1985**, *61*, 733.
(21) Doi, M.; Edwards, S. F. *The Theory of Polymer Dynamics*; Clarendon Press: Oxford, 1986.
(22) A sticker could make an attempt to look for a core of a new micelle by combining an activated slippage along its tube with tube leakage. The typical spacial sticker displacement due to the slippage is $\Delta R \sim \sqrt{a_e \Delta L}$, where $\Delta L \sim a_e(xl/N_e)^{1/2}$ is the displacement along the confining tube accompanied by the elastic energy increment on the order of k_BTx. Using eq 48, we find that $\Delta R < a_e x$ if $m^2 > N_e$, which is assumed to be the case (see eq 46). Hence, the volume searched by the sticker is indeed nearly spherical.
(23) Another possibility, not considered here, is that micelles form a regular positional superstructure.
(24) If the spacers are not extremely long, $l \ll m^5$; this condition ensures that the deformation energy $\Delta\mathcal{F}$ is high even at $\phi \sim 1$: $\Delta\mathcal{F}/(k_BT) \gg 1$.

MA0117965